

1 Eruptive history and $^{40}\text{Ar}/^{39}\text{Ar}$ geochronology of the Milos volcanic 2 field, Greece

3
4 Xiaolong Zhou¹, Klaudia Kuiper¹, Jan Wijbrans¹, Katharina Boehm¹, Pieter Vroon¹

5 ¹Department of Earth Sciences, VU University Amsterdam, De Boelelaan 1085, 1081 HV Amsterdam, The Netherlands.

6 *Correspondence to:* Xiaolong Zhou (z.x.l.zhou@vu.nl)

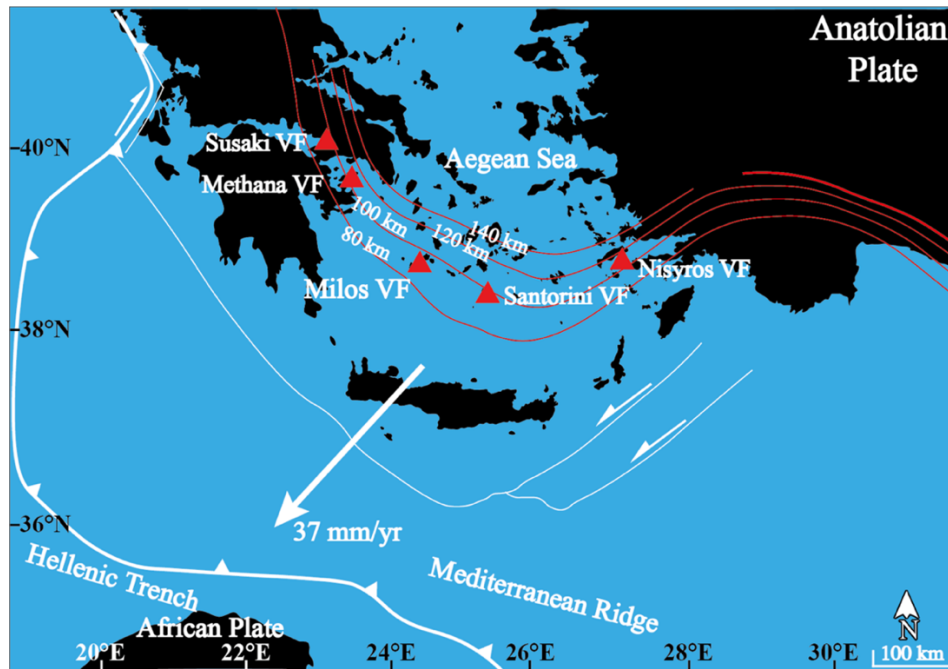
7 **Abstract.** High-resolution geochronology is essential for determining the growth-rate of volcanoes, which is one of the key
8 factors for establishing the periodicity of volcanic eruptions. However, there are less high-resolution eruptive histories ($>10^6$
9 years) determined for long-lived submarine arc volcanic complexes than for subaerial complexes, since submarine volcanoes
10 are far more difficult to observe than subaerial ones. In this study, high-resolution geochronology and major element data are
11 presented for Milos Volcanic Field (VF) in the South Aegean Volcanic Arc, Greece. The Milos VF has been active for over 3
12 Ma, and the first two million years of its eruptive history occurred in a submarine setting that has been emerged above sea
13 level. The long submarine volcanic history of the Milos VF makes it an excellent natural laboratory to study the growth-rate
14 of a long-lived submarine arc volcanic complex. This study reports twenty-one new high-precision $^{40}\text{Ar}/^{39}\text{Ar}$ ages and major
15 element compositions for eleven volcanic units of the Milos VF. This allows us to divide the Milos volcanic history into at
16 least three periods of different long-term volumetric volcanic output rate (Q_e). Period I (submarine, ~ 3.3 -2.13 Ma) and III
17 (subaerial, 1.48 Ma-present) have low Q_e of $0.9 \pm 0.5 \times 10^{-5} \text{ km}^3 \cdot \text{yr}^{-1}$ and $0.25 \pm 0.05 \times 10^{-5} \text{ km}^3 \cdot \text{yr}^{-1}$, respectively. Period II
18 (submarine, 2.13 - 1.48 Ma) has a 3-12 times higher Q_e of $3.0 \pm 1.7 \times 10^{-5} \text{ km}^3 \cdot \text{yr}^{-1}$. The Q_e of the Milos VF is 2-3 orders of
19 magnitude lower than the average for rhyolitic systems and continental arcs.

20 1 Introduction

21 Short-term eruptive histories and compositional variations of lavas and pyroclastic deposits of many arc volcanic fields are
22 well established. However, high-resolution eruptive histories that extend back $> 10^5$ - 10^6 years have been determined only for
23 a handful of long-lived subaerial arc volcanic complexes. Some examples are: Mount Adams (Hildreth and Lanphere, 1994),
24 Tatará–San Pedro (Singer et al., 1997), Santorini (Druitt et al., 1999), Montserrat (Cole et al., 2002), Mount Baker (Hildreth
25 et al., 2003a), Katmai (Hildreth et al., 2003b), and Ceboruco–San Pedro (Frey et al., 2004). To establish the growth-rate of
26 volcanic complexes and disentangle the processes responsible for the eruption, fractionation, storage, and transport of magmas
27 over time, comprehensive geological studies are required. These include detailed field mapping, sampling, high-resolution
28 geochronology and geochemical analysis. Based on these integrated studies, the growth-rate of volcanoes can be determined
29 to establish the periodicity of effusive and explosive volcanism.

30 The Milos Volcanic Field (VF) is a long-lived volcanic complex that has been active for over 3 Ma. The Milos VF erupted for
31 a significant part of its life below sea level, similar to the other well studied volcanic structures in the eastern Mediterranean
32 (Fytikas et al., 1986; Stewart and McPhie, 2006). The eruptive history of the Milos VF has been examined with a broad range
33 of chronostratigraphic techniques such as K-Ar, U-Pb, fission track, ^{14}C and biostratigraphy (e.g. Angelier et al., 1977, Fytikas
34 et al., 1976, 1986, Traineau and Dalabakis, 1989, Matsuda et al., 1999, Stewart and McPhie, 2006, Van Hinsbergen et al., 2004
35 and Calvo et al., 2012). However, most of the published ages have been measured using the less precise K-Ar or fission track
36 methods, and modern, high precision $^{40}\text{Ar}/^{39}\text{Ar}$ ages for the Milos VF have not been published so far. In this study, (1) we
37 provide high-precision $^{40}\text{Ar}/^{39}\text{Ar}$ geochronology of key volcanic units of the Milos VF and (2) refine the stratigraphic

38 framework of the Milos VF with the new high-precision $^{40}\text{Ar}/^{39}\text{Ar}$ ages and major element composition. (3) We also quantify
39 and constrain the compositional and volumetric temporal evolution of volcanic products of the Milos VF.



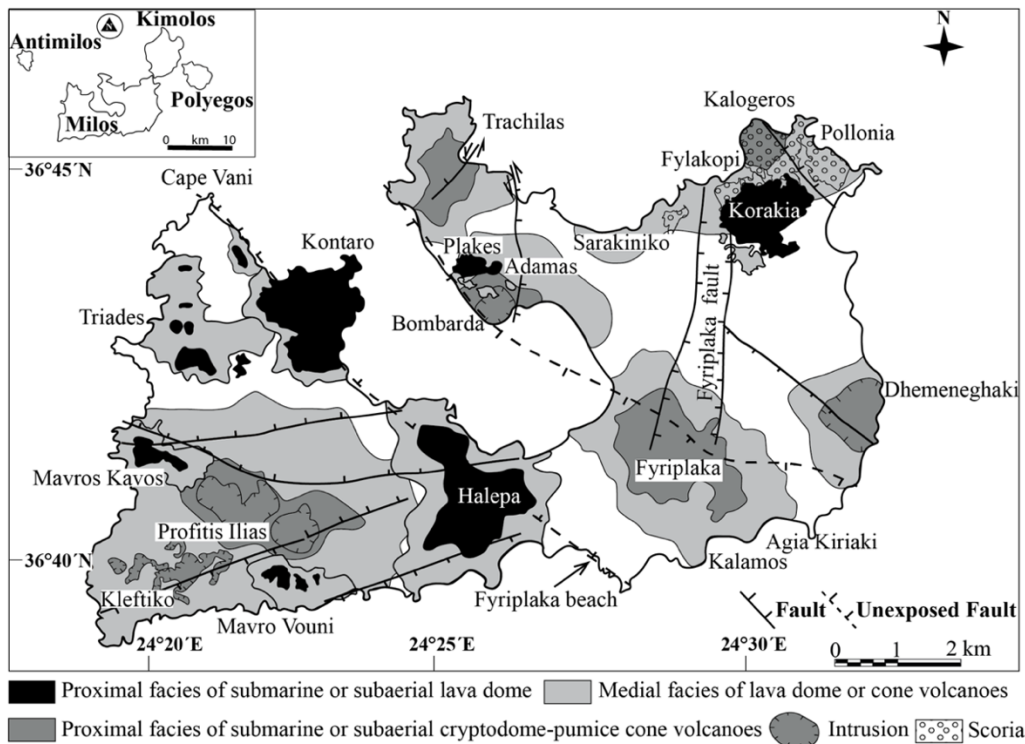
40
41 **Figure 1. Map of the South Aegean Volcanic Arc (SAVA). Red triangles indicate Volcanic Fields (VF): Susaki, Methana and Milos**
42 **VFs in the western SAVA, Santorini VF in the centre and Nisyros VF in the eastern SAVA. Red contour lines show the depth to**
43 **the Benioff zone (Hayes et al., 2018). The white arrow represents the GPS-determined plate velocity of the Aegean microplate**
44 **relative to the African plate from Doglioni et al. (2002).**

45 1.1 Geological setting

46 The Milos VF is part of the South Aegean Volcanic Arc (SAVA), an arc which was formed in the eastern Mediterranean by
47 subduction of the African plate beneath the Aegean microplate (Figure 1, Nicholls, 1971; Spakman et al., 1988; Duermeijer et
48 al., 2000; Pe-Piper and Piper, 2007; Rontogianni et al., 2011). The present-day Benioff zone is located approximately 90 km
49 underneath Milos (Hayes et al., 2018). The upper plate is influenced by extensional tectonics (e.g. McKenzie, 1978; Pe-Piper
50 and Piper, 2013), which is evident on the island of Milos as horst and graben structures (Figure 2).

51 The Milos VF is exposed on the islands of the Milos archipelago: Milos, Antimilos, Kimolos and Polyegos. The focus of this
52 study is Milos which has a surface area of 151 km². The geology and volcanology of Milos have been extensively studied in
53 the last 100 years. The first geological map was produced by Sonder (1924). This work was extended by Fytikas et al. (1976)
54 and Angelier et al. (1977) and the subsequent publications of Fytikas et al. (1986) and Fytikas (1989). Interpretations based on
55 volcanic facies of the complete stratigraphy were made by Stewart and McPhie (2003, 2006). More detailed studies of single
56 volcanic centres (e.g. Bombarda volcano and Fyriplaka complex) were published by Campos Venuti and Rossi (1996) and
57 Rinaldi et al. (2003). Milos has also been extensively studied for its epithermal gold mineralization, summarized by Alfieris
58 et al. (2013). Milos was known during the Neolithic period for its export of high-quality obsidian. Today the main export
59 product is kaolinite mined from hydrothermally altered felsic volcanic units in the centre of the island (e.g. Alfieris et al.,
60 2013).

61 The geology of Milos can be divided into four main units: (1) metamorphic basement, (2) Neogene sedimentary rocks, (3)
62 volcanic sequences and (4) the alluvial cover. The metamorphic basement crops out at the southwest, south and southeast of
63 Milos (Figure 3) and is also found as clasts in many volcanic units. The metamorphic rocks include lawsonite-free jadeite
64 eclogite, lawsonite eclogite, glaucophane schist, quartz-muscovite-chlorite and chlorite-amphibole schist (Fytikas et al., 1976,
65 1986; Grasemann et al., 2018; Kornprobst et al., 1979). The exposed units belong to the Cycladic Blueschist Unit (Lower
66 Cycladic nappe), whereas eclogite pebbles in the phreatic eruption products called “green lahar” by Fytikas (1977) are derived
67 from the Upper Cycladic Nappe (Grasemann et al., 2018).



68

69

70

71

Figure 2. Distribution of the proximal and medial facies of the submarine pumice cone/cryptodome volcanoes, submarine, submarine-subaerial and subaerial domes and rhyolitic complexes (tuff cone and associated lava) of Milos, modified after Fytikas et al. (1986) and Stewart and McPhie (2006). The distal facies of Stewart and McPhie (2006) is not shown.

72

73

74

75

76

77

78

79

80

81

82

On top of this metamorphic basement, Neogene fossiliferous marine sedimentary rocks were deposited (e.g. Van Hinsbergen et al. 2004). This sedimentary sequence can be divided into a lower unit A and upper unit B that is unconformably overlain by volcanoclastic sediments (Van Hinsbergen et al., 2004). Unit A is 80 m thick and consists of fluvatile-lacustrine, brackish and shallow marine conglomerate, sandstone, dolomite and limestone. Unit B is 25-60 m thick and consists of sandstone overlain by a succession of alternating marls and sapropels, suggesting a deeper marine setting (Van Hinsbergen et al., 2004). Five volcanic ash layers that contain biotite are found in this Neogene sedimentary sequence, either suggesting that volcanic eruptions in small volume already occurred in the Milos area or that these ash layers are derived from larger eruptions of volcanic centres further away from Milos (van Hinsbergen et al., 2004). Age determinations by bio-magneto- and cyclostratigraphy suggested that deposition of Unit A started at approximately 5 Ma, and that Milos subsided 900 m in 0.6 Ma (Van Hinsbergen et al. 2004) due to extension. This subsidence happened ca 1.0-1.5 Ma before the onset of the main phase of Pliocene- recent volcanism on Milos.

83

84

85

86

87

88

89

90

91

The Pliocene-recent volcanic sequence of Milos has been subdivided into different units by Angelier et al. (1977) and Fytikas et al. (1986). In addition, Stewart and McPhie (2006) provided a detailed facies analysis of the different volcanic units. The subdivision by Angelier et al. (1977) is not constrained well due to their limited amount of age data. The subdivision of volcanic units by Fytikas et al. (1986) and facies descriptions of Stewart and McPhie (2006) are summarized below. It is important to note that according to Stewart and McPhie (2006), the five volcanic cycles described by Fytikas et al. (1986) are difficult to match with existing age data and the continuous progression in volcanic construction (Fig. 4). For example, the first phase of Fytikas et al. (1986), the Basal Pyroclastic Series, contains the large pumice cone-cryptodome volcanoes according to Stewart and McPhie (2006). Two of these pumice-cone cryptodome volcanoes are much younger and intercalated between the Complex of Domes and Lava Flows (CDLF) of Fytikas et al. (1986).

92

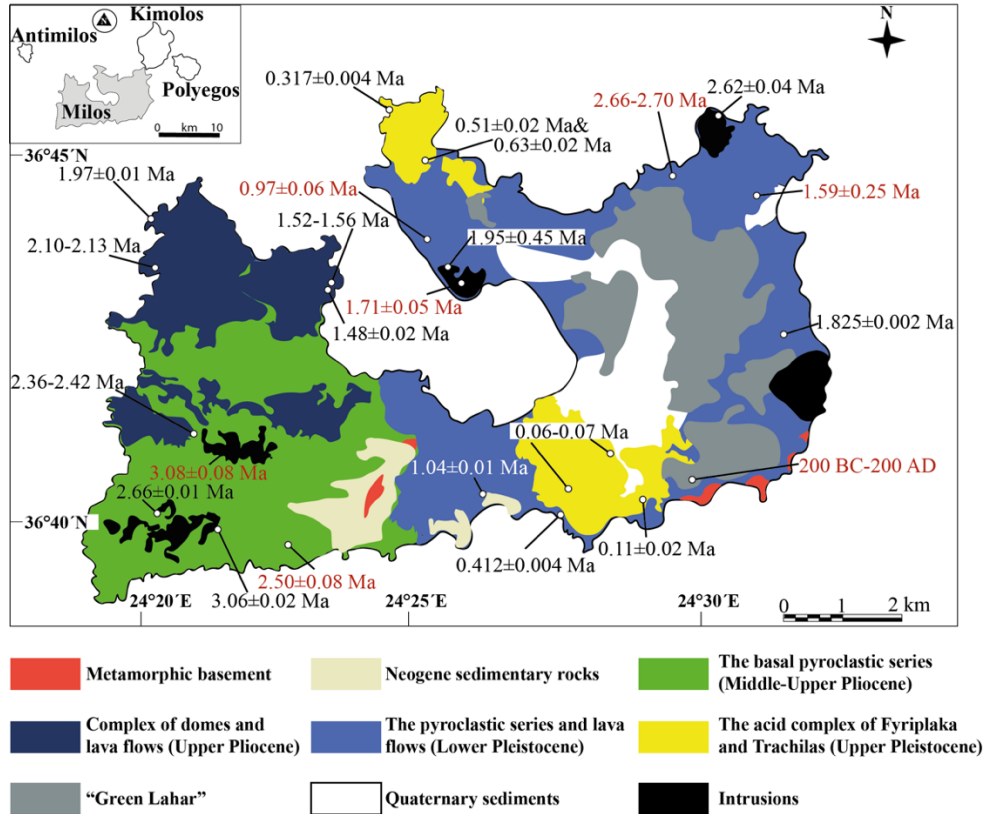
93

94

95

The first volcanic unit deposited in the Milos area is the Basal Pyroclastic Series (BPS) (Fytikas et al., 1986) or submarine felsic cryptodome-pumice cone volcanoes (Stewart and McPhie, 2006, Figure 2-4). This unit consists of thickly bedded pumice breccia with a rhyolitic-dacitic composition. These rhyolites-dacites are aphyric or contain quartz-feldspar±biotite phenocrysts. Graded sandstone and bioturbated and fossil rich (in-situ bivalve shells) mudstone are intercalated, indicating a marine

96 environment and a water depth of several hundreds of meters (e.g. Stewart, 2003; Stewart and McPhie, 2006), whereas later
 97 degassed magmas with a similar composition intruded as sills and cryptodomes. The BPS has been strongly affected by
 98 hydrothermal fluids, especially the proximal deposits (e.g. Kiliias et al., 2001).



99
 100 **Figure 3. Simplified geological map of Milos with our ⁴⁰Ar/³⁹Ar ages and sample locations of key volcanic deposits, modified after**
 101 **Stewart and McPhie (2006) and Grasmann et al. (2018). The stratigraphic units of Milos are from Fytikas et al. (1986). Age data**
 102 **from this study are in black, published ages are shown in red (Angelier et al., 1977, Fytikas et al., 1986, Traineau and Dalabakis,**
 103 **1989, and Stewart and McPhie, 2006). The "Green Lahar" (Fytikas, 1977) consists of deposits from multiple phreatic explosions**
 104 **and contains fragments of metamorphic, sedimentary and volcanic rocks.**

105 The second volcanic unit was named the Complex of Domes and Lava Flows (CDLF, Fytikas et al., 1986) and the volcanic
 106 facies of this unit are described as the submarine dacitic and andesitic domes by Stewart and McPhie (2006). This phase of
 107 effusive submarine volcanism was predominantly andesitic/dacitic in composition and produced microcrystalline rocks with
 108 phenocrysts of pyroxene, amphibole, biotite and plagioclase. The eruption centres were mainly located along NNE faults and
 109 formed up to 300 m thick deposits extending over areas of 2.5 to 10 km² around the eruption centres. In the north-eastern part
 110 of Milos, an andesitic scoria cone provided scoria lapilli and bombs to deeper water settings. Sandstone intercalated in the
 111 CDLF contains both igneous and metamorphic minerals suggesting input from the basement. Rounded pebbles of rhyolite and
 112 dacite indicate that some of the volcanic deposits were above sea level, or in very shallow, near shore environments (e.g.
 113 Stewart and McPhie, 2006).

114 The third volcanic unit is called the Pyroclastic Series and Lava Domes (PSLD) by Fytikas et al. (1986) and belongs to
 115 submarine-to-subaerial dacitic and andesitic lava domes of Stewart and McPhie (2006). This highly variable group is
 116 dominated by rhyolitic, dacitic and andesitic lavas, domes, pyroclastic deposits and felsic pumiceous sediments (Stewart and
 117 McPhie, 2006). Thickness varies between 50-200 m, and the deposits are located in the eastern and northern parts of Milos
 118 (Figure 2 and 3). The initial pyroclastic layers were subaqueously deposited and the extrusion of a dome resulted in the
 119 deposition of talus around the margins by mass flow. On top of the dome sand- and siltstone with fossils (Ostrea fossil
 120 assemblage) and traction-current structures suggest that the top of the dome was above wave base. The youngest deposits of
 121 this unit are dacitic and andesitic lavas and domes. These domes generated subaerial block-and-ash flow and surge deposits.
 122 Paleosols within these deposits are a clear indicator that some areas were above sea level. The last unit of the PSLD is

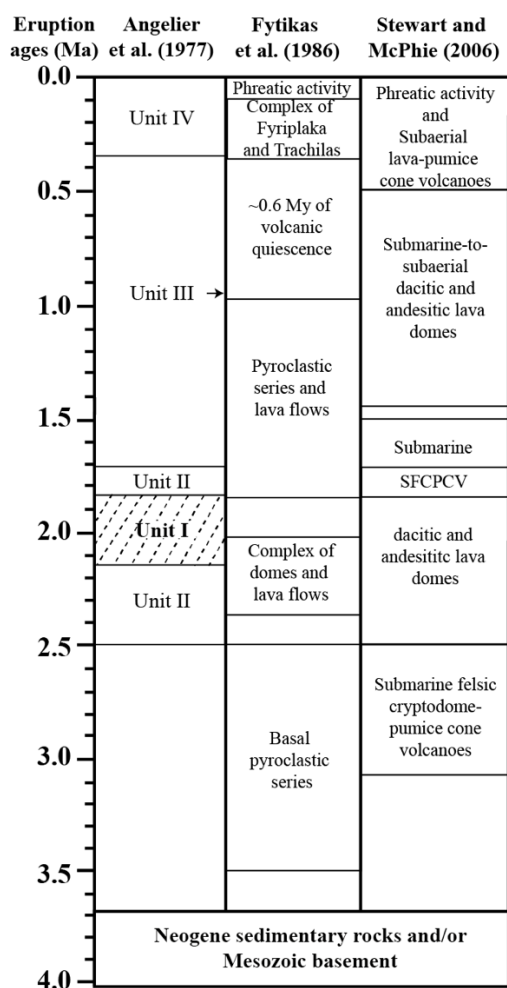
123 represented by large subaerial rhyolitic lava that contains quartz and biotite phenocrysts and is found near Halepa in the south-
 124 central part of Milos.

125 **Table 1. Published eruption ages of stratigraphic units of the island of Milos**

Stratigraphy	Sample	Mineral	Location	Petrology	K ₂ O (wt.%)	Age (Ma)	± 1σ	Reference
Unit IV	Angelier_1	Unknown	Fyriplaka	Rhyolite	-	-	-	
Unit III	Angelier_2	Unknown	Halepa	Rhyolite	2.44	0.95	0.06	
Unit II	Angelier_3	Unknown	Triades	Dacite	1.47	1.71	0.08	Angelier et al. (1977)
	Angelier_4	Unknown	Kleftico	Andesite	1.77	2.33	0.09	
	Angelier_5	Unknown	Kleftico	Andesite	1.45	2.50	0.09	
Unit I	Angelier_6	Unknown	Adamas	Rhyolite	2.90	2.15	0.08	
	Angelier_7	Unknown	Dhemenehaki	Rhyolite	2.75	1.84	0.08	
Phreatic activity	Gif-7358&7359	Carbonized wood	Agia Kiriaki	Lahar deposits	-	200 BC-200 AD		Trainau and Dalabakis (1989)
CFT	M196	Unknown	Fyriplaka	Rhyolite	2.9	0.09	0.02	Fytikas et al. (1976, 1986)
	M194	Unknown	Fyriplaka	Rhyolite	2.85	0.14	0.03	
	M168	Unknown	Trachilas	Rhyolite	3.91	0.37	0.09	
	M-48	Biotite	NW of Filiplaka	Rhyolite	6.41	0.48	0.05	
PSLD	M-OB1	Groundmass	N of Dhemenehaki	Obsidian	2.53	0.88	0.18	Fytikas et al. (1976, 1986)
	M27	Unknown	Plakes	Dacite	1.87	0.97	0.06	
	M-OB2	Groundmass	Bombarda	Obsidian	2.73	1.47	0.05	
	M103	Unknown	near Pollonia	Andesite	1.87	1.59	0.25	
	M146	Unknown	1km NW of Adamas	Rhyolite	3.09	1.71	0.05	
	M110	Unknown	Sarakiniko	Dacite	2.57	1.85	0.10	Matsuda et al. (1999)
	MI-1	Lava	Plakes	Dacite	2.07	0.80	0.10	
	MI-4	Lava	Plakes	Dacite	2.32	1.20	0.10	
	MIL130	Zircon	Triades	Dacite	-	1.44	0.08	Stewart and McPhie (2006)
	Fission track1	Groundmass	Adamas	Obsidian	-	1.54	0.18	Bigazzi and Radi (1981)
Fission track2	Groundmass	Bombarda	Obsidian	-	1.57	0.15		
Fission track3	Groundmass	Bombarda-Adamas	Obsidian	-	1.57	0.12	Arias et al. (2006)	
Fission track3	Groundmass	Dhemenehaki	Obsidian	-	1.60	0.06		
CDLF	M1	Unknown	Aghios, near Triades	Rhyolite	3.32	2.04	0.09	Fytikas et al. (1976, 1986)
	M66	Unknown	~1 km NW of Adamas	Dacite	2.61	2.03	0.06	
	M156	Unknown	Angathia, near Triades	Dacite	2.84	2.38	0.10	
	MIL243	Zircon	Triades	Dacite	-	2.18	0.09	Stewart and McPhie (2006)
BPS	MIL365	Zircon	Filakopi	Rhyolite	-	2.66	0.07	Stewart and McPhie (2006)
	MIL343	Zircon	Kalogeros cryptodome	Dacite	-	2.70	0.04	
	M164	Unknown	Kleftico	Rhyolite	2.84	3.08	0.08	Fytikas et al. (1976, 1986)
	M163	Unknown	Kleftico	Andesite	1.18	3.50	0.14	

126 Angelier et al. (1977) do not provide sample names, only numbers for the sample locations. Here the location is given after “Angelier_”
 127 (Angelier et al. 1977, their Fig. 3). Abbreviations: BPS=Basal pyroclastic series; CDLF=Complex of domes and lava flows;
 128 PSLD=Pyroclastic series and lava domes; CTF=Complexes of Trachilas and Fyriplaka. See more details in Figure. 4.

129 The fourth unit consists of the subaerially constructed rhyolitic Complexes of Trachilas and Fyriplaka (CTF) (Fytikas et al.,
 130 1986), which Stewart and McPhie (2006) interpreted as subaerial rhyolitic lava-pumice cones. These two volcanic complexes
 131 are built from rhyolitic pumice deposits and lavas that contain quartz and biotite phenocrysts (10-20 modal %). The deposits
 132 have a maximum thickness of 120 m and decrease to several meters thickness in the distal parts. Basement-derived schist is
 133 found as lithic clasts (Fytikas et al., 1986). In addition, the Kalamos rhyolitic lava dome, which outcrops on the southern coast
 134 of Milos, produced lava that spread westwards to the Fyriplaka beach (Figure 2). This lava belongs to this fourth phase and is
 135 probably derived from an older volcano and not the Fyriplaka complex (Campos Venuti and Rossi, 1996).
 136 The fifth volcanic unit comprises deposits from phreatic activity, especially in the northern part of the Zefiria Graben and near
 137 Agia Kiriaki (Figure 2 of Stewart and McPhie, 2006). Many overlapping craters are surrounded by lithic breccias that are
 138 composed of variably altered metamorphic basement clasts and volcanic clasts. This phreatic activity has continued into
 139 historic times (Trainau and Dalabakis, 1989). Fytikas et al. (1986) referred to this unit as “green lahar”, although it indicated
 140 that this deposit is not a lahar but the product of phreatic eruptions in the last 0.2 Ma.



141
 142 **Figure 4. Previous proposed stratigraphic frameworks for Milos by Angelier et al. (1977), Fytikas et al. (1986) and Stewart and**
 143 **McPhie (2006). Volcanic unit II of Angelier et al. (1977) contains unit I. Stewart and McPhie (2006) described the volcanic faces of**
 144 **Milos mainly based on the geochronological works of Angelier et al. (1977) and Fytikas et al. (1986). Abbreviation:**
 145 **SFCPCV=Submarine felsic cryptodome-pumice cone volcanoes.**

146 **1.2 Previous geochronological studies**

147 Previous geochronological work is summarised in Table 1. Angelier et al. (1977) reported six K-Ar ages (0.95-2.50 Ma). These
 148 ages were used in combination with field observations to divide the Milos volcanic succession into four units. However, the
 149 samples from Fyriplaka, the fourth unit, were too young to be dated by Angelier et al. (1977). Fytikas et al. (1976, 1986)
 150 published 16 K-Ar ages for Milos (0.09-3.50 Ma) including an age of 0.09-0.14 Ma for the Fyriplaka complex. Fytikas et al.
 151 (1986) also obtained 3 K-Ar ages for Antimilos (0.32 ± 0.05 Ma), Kimolos (3.34 ± 0.06 Ma) and Polyegos (2.34 ± 0.17 Ma).

152 Trainau and Dalabakis (1989) dated the very young phreatic deposits by ^{14}C dating and found ages between 200 BC and 200
153 AD. Matsuda et al. (1999) published two K-Ar ages of 0.8 ± 0.1 (MI-1) and 1.2 ± 0.1 Ma (MI-4) for the Plakes dome that was
154 also studied by Fytikas et al. (1986). Bigazzi and Radi (1981) published two fission track ages of 1.54 ± 0.18 and 1.57 ± 0.15
155 Ma for obsidians of Bombarda-Adamas and Demenaghaki, respectively. Later fission track studies by Arias et al. (2006) (1.57
156 ± 0.12 and 1.60 ± 0.06 Ma) confirmed these ages. The fission track ages are younger than the K-Ar ages given by Angelier et
157 al. (1977; 1.84 ± 0.08 Ma for Demenaghaki) and Fytikas et al. (1986; 1.71 ± 0.05 Ma for Bombarda). In the most recent
158 geochronological study of the Milos VF, Stewart and McPhie (2006) published 4 SHRIMP U/Pb zircon ages: Triades dacite
159 facies (1.44 ± 0.08 and 2.18 ± 0.09 Ma), Kalogeros cryptodome (2.70 ± 0.04 Ma) and the Fylakopi Pumice Breccia ($2.66 \pm$
160 0.07 Ma). All uncertainties reported here are one standard deviation uncertainties as reported in the original publications,
161 except for the ^{14}C ages for which uncertainties were not specified.

162 **2 Methods**

163 **2.1 Mineral separation and sample preparation**

164 Samples were collected from all major volcanic units on Milos island based on the studies of Fytikas et al. (1986), Stewart and
165 McPhie (2006) and our own observations in the field. Photos of the sample locations and thin sections can be found in
166 supplementary material I. Approximately 2 kg of fresh pumice clasts or lava was sampled from each unit. Samples were cut
167 into $\sim 5\text{ cm}^3$ cubes using a diamond saw to remove potentially altered surfaces and obtain the fresh interior parts. These cubes
168 were ultra-sonicated for 30 minutes in demi-water to remove dust and seawater and dried in an oven overnight at $50\text{ }^\circ\text{C}$. Dry
169 sample cubes were crushed in a steel jaw crusher, and this fraction was split into two portions of roughly equal size. One of
170 them was powdered in an agate shatter box and agate ball mill to a grain size of less than $2\text{ }\mu\text{m}$ for the major-element analysis.
171 The second fraction was sieved to obtain a grain size of 250-500 μm for $^{40}\text{Ar}/^{39}\text{Ar}$ dating.

172 Heavy liquids density separation techniques (IJlst, 1973) were used to purify mineral separates (groundmass, biotite, amphibole)
173 required for the $^{40}\text{Ar}/^{39}\text{Ar}$ dating. Different densities of heavy liquids were used to obtain groundmass ($2700 \leq \rho \leq 3000\text{ kg.m}^{-3}$),
174 biotite ($2900 \leq \rho \leq 3100\text{ kg.m}^{-3}$) and/or amphibole ($\sim 3100 \leq \rho \leq 3200\text{ kg.m}^{-3}$). A Franz Isodynamic Magnetic separator was
175 used to remove the magnetic minerals from the non-magnetic minerals and groundmass. The samples for $^{40}\text{Ar}/^{39}\text{Ar}$ analysis
176 were purified by handpicking under a binocular optical microscope to select mineral grains without visible alteration and
177 inclusions.

178 **2.2 $^{40}\text{Ar}/^{39}\text{Ar}$ dating**

179 The mineral and groundmass samples were wrapped in either 6- or 9-mm aluminium foil and packed in 20 mm aluminium
180 cups, that were vertically stacked. Based on stratigraphy and previous geochronological constraints >1 Ma samples and the <1
181 Ma samples were irradiated for 7 and 1 hours respectively in irradiation batches VU108 and VU110 in the Cadmium-Lined
182 in-Core Irradiation Tube (CLICIT) facility of the Oregon State University Training Research, Isotopes, General Atomics
183 (TRIGA) reactor. The neutron flux for all irradiations was monitored by standard bracketing using the Drachenfels sanidine
184 (DRA; 25.52 ± 0.08 Ma, modified from Wijbrans et al., 1995 and calibrated relative to Kuiper et al., 2008) and Fish Canyon
185 Tuff sanidine (FCs; 28.201 ± 0.023 Ma, Kuiper et al., 2008) with Min et al. (2000) decay constants.

186 In total, 24 samples (8 groundmasses, 15 biotites and 2 amphiboles, for sample G15M0026 both biotite and amphibole were
187 analysed) were measured by either $^{40}\text{Ar}/^{39}\text{Ar}$ fusion and/or incremental heating techniques. For incremental heating
188 experiments, 80-100 grains per sample were loaded into a 25-hole (surface per hole $\sim 36\text{ mm}^2$) copper tray together with single
189 grain standards in $\sim 12\text{ mm}^2$ holes. The tray was prebaked in vacuum (10^{-5} - 10^{-6} mbar) at $250\text{ }^\circ\text{C}$ overnight to remove
190 atmospheric argon and subsequently baked overnight at $120\text{ }^\circ\text{C}$ in the ultra-high vacuum sample chamber ($<5 \times 10^{-9}$ mbar) and
191 purification system connected to a Thermo Scientific Helix MC mass spectrometer.

192 Samples and standards were heated with a focused laser beam at 8 % power using a 50W CW CO₂ laser. The released gas was
 193 cleaned by exposure to a cold trap cooled by a Lauda cooler at -70 °C, a SAES NP10 at 400 °C, Ti sponge at 500 °C and cold
 194 SAES ST172 Fe-V-Zr sintered metal. The five isotopes of argon were measured simultaneously on five different collectors:
 195 ⁴⁰Ar on the H2-Faraday, ³⁹Ar on the H1-Faraday or the H1-CDD, ³⁸Ar on the AX-CDD, ³⁷Ar on the L1-CDD and ³⁶Ar on the
 196 L2-CDD for 15 cycles with 33 seconds integration time (CDD: compact discrete dynodes). The Faraday cups on H2 and H1
 197 were equipped with 10¹³ Ω amplifiers. Procedural blanks were measured every 2 or 3 analyses in different sequences, and air-
 198 shots were measured every 8-12 hours to correct the instrumental mass discrimination. Gain between different collectors was
 199 monitored by measuring CO₂ on mass 44 in dynamic mode on all collectors. Gain was generally stable over periods of weeks.
 200 Note that because samples, standards and air calibration runs are measured during the same period, gain correction does not
 201 substantially change the final age results. The raw mass spectrometer data output was converted by an in-house designed Excel
 202 macro script to be compatible with the ArArCalc 2.5 data reduction software (Koppers, 2002). The ⁴⁰Ar/³⁶Ar atmospheric air
 203 value of 298.56 from Lee et al. (2006) is used in the calculations. The correction factors for neutron interference reactions are
 204 (2.64 ± 0.02) x10⁻⁴ for (³⁶Ar/³⁷Ar)_{Ca}, (6.73 ± 0.04) x10⁻⁴ for (³⁹Ar/³⁷Ar)_{Ca}, (1.21 ± 0.003) x10⁻² for (³⁸Ar/³⁹Ar)_K and (8.6 ± 0.7)
 205 x10⁻⁴ for (⁴⁰Ar/³⁹Ar)_K. All uncertainties are quoted at the 1σ level and include all analytical errors (i.e. blank, mass
 206 discrimination and neutron interference correction and analytical error in J-factor, the parameter associated with the irradiation
 207 process).

208 A reliable plateau age is defined as experiments with at least 3 consecutive steps overlapping at 2-sigma, containing >50% of
 209 the ³⁹Ar_K, a Mean Square Weighted Deviate (MSWD) value <2.5, and with a ⁴⁰Ar/³⁶Ar inverse isochron intercept that does not
 210 deviate from atmospheric argon at 2-sigma. All the inverse isochron ages used the same steps as used in the weighted mean
 211 ages, and all relevant analytical data for the age calculations following standard practices (Schaen et al., 2020) can be found
 212 in supplementary material II.

213 2.3 Whole-rock major element analysis by XRF

214 Major-element concentrations were measured by X-ray fluorescence spectroscopy (XRF) on a Panalytical AxiosMax. A
 215 Panalytical Eagon2 was used to create 40mm fused glass beads of Li₂B₄O₇/LiBO₂ (65.5:33.5%, Johnson & Johnson
 216 Spectroflux 110) with a 1:6 dilution sample-flux ratio that were molten at 1150 °C. Sample powders were ignited at 1000 °C
 217 for 2 hours to determine loss on ignition (LOI) before being mixed with the Li₂B₄O₇/LiBO₂ flux. Interference corrected spectra
 218 intensities were converted to oxide-concentrations against a calibration curve consisting of 30 international standards. The
 219 precision, expressed as the coefficient of variation (CV), is better than 0.5%. The accuracy, as measured on the international
 220 standards AGV-2, BHVO-2, BCR-2 and GSP-2 was better than 0.7% (1 RSD) (supplementary material III).

221 2.4 Eruption volume calculation

222 The minimum and/or maximum eruption volume of each volcano during each eruption period is derived from the ranges of
 223 thickness and surface areas that are reported in Campos and Rossi (1996) and Stewart and McPhie (2006). We converted these
 224 volumes to Dense Rock Equivalent (DRE) based on the magma type of different deposits. This analysis only includes the
 225 onshore deposits and results in a smaller estimate for larger pyroclastic volumes. The DRE volume is calculated using the
 226 equation of Croweller et al. (2012):

$$227 \quad DRE (km^3) = \frac{tephra \text{ vol } (km^3) \times tephra \text{ density } (kg/m^3)}{magma \text{ density } (kg/m^3)}$$

228 Tephra density is assumed to be 1000 kg/m³ (Croweller et al., 2012). Magma density varies depending on the magma type.
 229 Here we used 2300 kg/m³ for rocks with a SiO₂ range of 65-77 wt.% and 2500 kg/m³ for all samples with SiO₂ < 65 wt.%.
 230 DRE corresponds to the unvesiculated erupted magma volume. Therefore, we did not convert the volume of some cryptodome
 231 and lavas from Profitis Ilias (G15M0017), Triades (G15M0021-24), Dhemenehaki (G15M0032B) and Halepa (G15M0013)

232 to the DRE since they contain less than 5% vesicles.

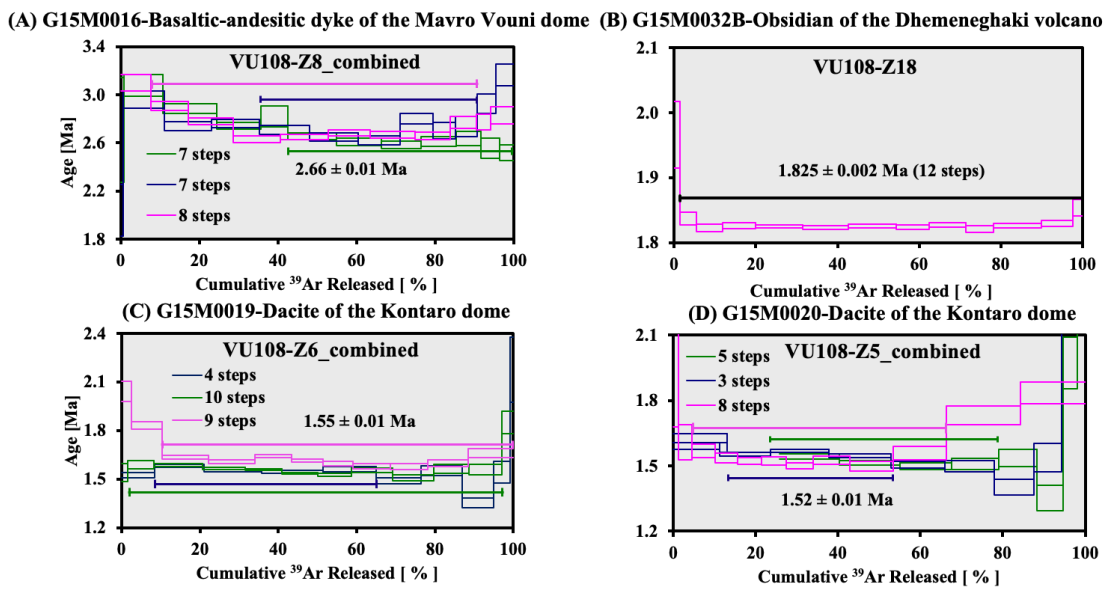
233 3 Results

234 3.1 $^{40}\text{Ar}/^{39}\text{Ar}$ age results

235 In this section, we present our groundmass, biotite and amphibole $^{40}\text{Ar}/^{39}\text{Ar}$ results for eleven volcanic units of Milos. The
236 $^{40}\text{Ar}/^{39}\text{Ar}$ ages range from 0.06 to 4.10 Ma and cover most of the major volcanic units of Milos. Table 2 and 3 show the
237 $^{40}\text{Ar}/^{39}\text{Ar}$ results of incremental heating steps and single grain fusion analyses, respectively. Note that the Irr-ID column in
238 these two Tables represents the irradiation ID of the analytical experiment (e.g. VU108-, VU110-) and the top right superscripts
239 (G, B, A, O) in the sample IDs (e.g., G15M0029^G, G15M0021^B) refer to groundmass, biotite, amphibole and obsidian.

240 3.1.1 Groundmass $^{40}\text{Ar}/^{39}\text{Ar}$ plateau and/or isochron ages

241 All groundmass samples yielding $^{40}\text{Ar}/^{39}\text{Ar}$ plateau and isochron ages with more than 50% $^{39}\text{Ar}_K$ and less than 2.5 MSWD
242 included in their age spectrum are shown in Figure 4 and reported in Table 2. The $^{40}\text{Ar}/^{36}\text{Ar}$ isochron intercepts do not deviate
243 from atmospheric argon at the 2-sigma level, unless stated otherwise (Table 3). Sample G15M0016 was collected from a dyke
244 at Kleftiko in the southwest of Milos (Figure 2). Three incremental heating experiments were performed on the groundmass
245 of this sample (Figure 5A). The first experiment (VU108-Z8a) produced a weighted mean age of 2.71 ± 0.02 Ma (MSWD
246 2.31; $^{39}\text{Ar}_K$ 79.6%; inverse isochron age 2.65 ± 0.10 Ma). The other two, VU108-Z8a_4 and VU108-Z8b_1, have plateau ages
247 of 2.61 ± 0.03 Ma (MSWD 0.93; $^{39}\text{Ar}_K$ 57.4%; inverse isochron age 2.69 ± 0.10 Ma) and 2.67 ± 0.01 Ma (MSWD 1.50; $^{39}\text{Ar}_K$
248 65.57%; inverse isochron age 2.55 ± 0.05 Ma), respectively. The three experiments are remarkably similar. Although the
249 amount of radiogenic ^{40}Ar is low (<20%), a combined age of 2.66 ± 0.01 Ma is considered to be the best estimate with a
250 relatively high MSWD value (2.51).



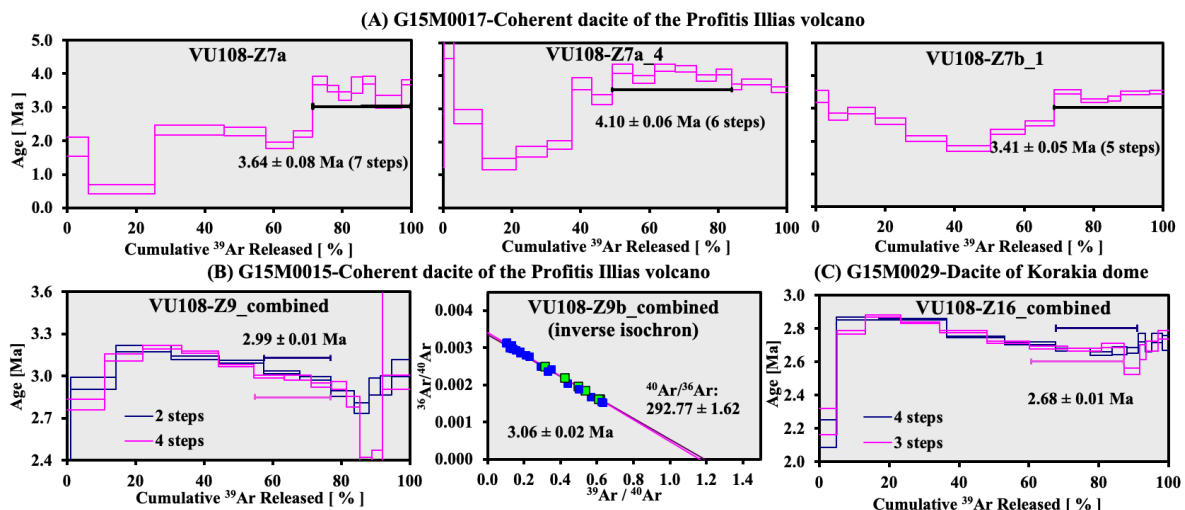
251
252 **Figure 5. Groundmass $^{40}\text{Ar}/^{39}\text{Ar}$ plateau ages for samples G15M0016 (A), G15M0032B (B), G15M0019 (C) and G15M0020 (D).**
253 **The Mavro Vouni dome (A), Dhemenehaki volcano (B) and Kontaro dacitic dome (C, D) are located in respectively the south-**
254 **western, north-eastern and eastern parts of Milos VF (see Fig. 2). Final age calculation is reported with 1σ errors. See the**
255 **individual steps of sample G15M0016, G15M0019 and G15M0029 in supplementary material II.**

256 Two lava samples, G15M0019 and G15M0020, were collected from Kontaro in north-eastern Milos (Figure 2). Three replicate
257 incremental heating step experiments on groundmass from sample G15M0019 (VU108-Z6a_4; VU108-Z6a_5 and VU108-
258 Z6b_1, Figure 5B) were performed that are not reproducible. Their plateau ages range from 1.55 Ma to 1.62 Ma with relatively
259 high MSWD (3.8-4.5), 56-95% of the total $^{39}\text{Ar}_K$, 34-53% of radiogenic ^{40}Ar , 0.88-1.02 of K/Ca and an atmospheric isochron
260 intercept of 297-315. We consider the isochron age from the last experiment (VU108-Z6b_1) as the reliable age (1.48 ± 0.02

261 Ma, MSWD 0.44) because its MSWD value is the only one smaller than 2.5 in this experiment, and therefore the best estimate
 262 for the eruption age. Three replicate incremental heating step experiments on groundmass from sample G15M0020 (VU108-
 263 Z5a_5; VU108-Z5b_1 and VU108-Z5b_2, Figure 5C) were analysed. These experiments are similar at the lower temperature
 264 heating steps. They produced statistically meaningful plateau ages ranging from 1.52-1.56 Ma with 41-62% of the total $^{39}\text{Ar}_K$,
 265 18-48% of radiogenic ^{40}Ar , 1.51-1.73 of K/Ca and an atmospheric isochron intercept of 295-300. Their combined weighted
 266 mean age is 1.54 ± 0.01 Ma (MSWD 3.06; $^{39}\text{Ar}_K$ 57.32%) with 25.31% of $^{40}\text{Ar}^*$.
 267 Sample G15M0032B (obsidian) was collected from a pumice cone volcano at Demeneghaki (Figure 2). One incremental
 268 heating experiment on this sample (VU108-Z18, Figure 5D) yielded a plateau age of 1.825 ± 0.002 Ma (MSWD 0.91; $^{39}\text{Ar}_K$
 269 98.6%). The $^{40}\text{Ar}^*$ is 93.86%. The inverse isochron age is identical to the weighted mean plateau age of 1.825 ± 0.002 Ma.
 270 The age of 1.825 ± 0.002 Ma is considered the best estimate for the eruption age of the Demeneghaki obsidian.

271 3.1.2 Groundmass $^{40}\text{Ar}/^{39}\text{Ar}$ plateau and/or isochron ages (25-40% $^{39}\text{Ar}_K$ released)

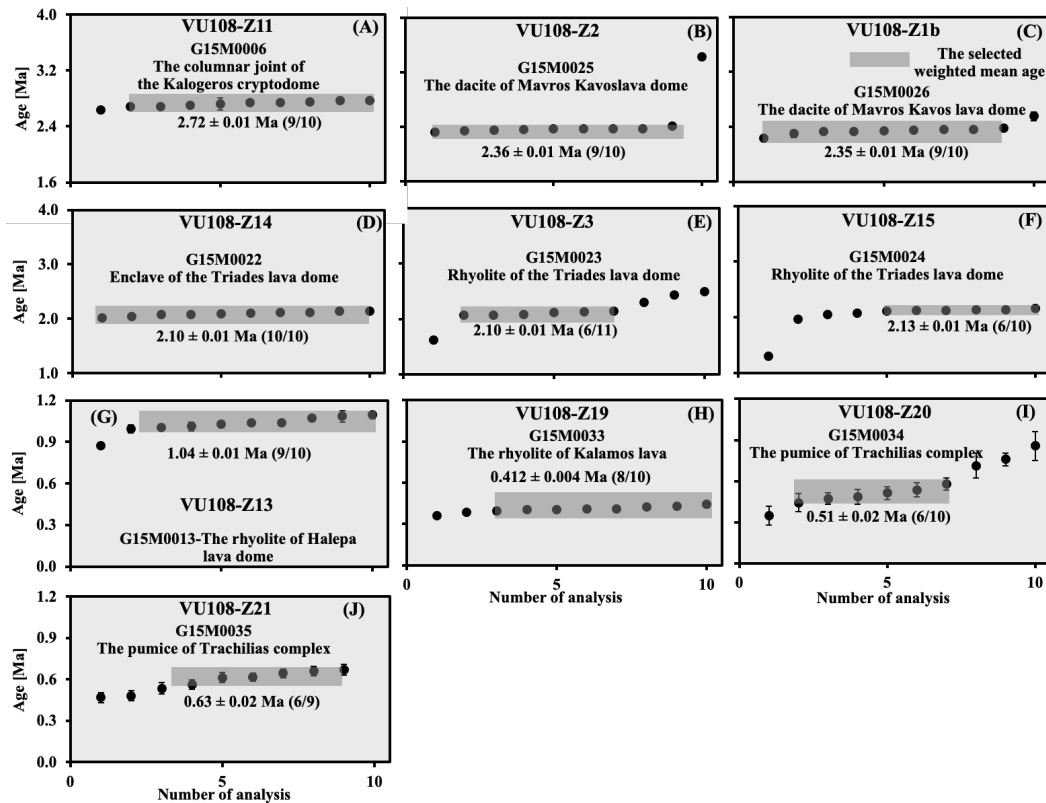
272 The results shown in Figure 5 did not yield weighted mean plateau ages according to standard criteria including $^{39}\text{Ar}_K > 50\%$,
 273 but still provide some useful age information. Sample G15M0017 was collected from a cryptodome of the Profitis Ilias
 274 volcano of southwestern Milos (Figure 2). Three replicate incremental heating experiments, VU108-Z7a, VU108-Z7a_4 and
 275 VU108-Z7b_1, have been performed on this sample which resulted in disturbed age spectra (Figure 6A). The consecutive
 276 lower temperature steps of all experiments define ages of <2.5 Ma, which is much younger than the ages of the submarine
 277 pyroclastic products of the lower series at Kleftiko and/or Profitis Ilias (3.0-3.5 Ma, Fytikas et al., 1986 and Stewart and
 278 McPhie, 2006). At the consecutive higher temperature heating steps, these experiments yielded 3.64 ± 0.08 Ma ($^{40}\text{Ar}/^{36}\text{Ar}$
 279 293.87 ± 4.77 ; VU108-Z7a), 4.10 ± 0.06 Ma ($^{40}\text{Ar}/^{36}\text{Ar}$ 298.44 ± 15.51 ; VU108-Z7a_4) and 3.41 ± 0.05 Ma ($^{40}\text{Ar}/^{36}\text{Ar}$ 295.97
 280 ± 7.34 ; VU108-Z7b_1). The total fusion and inverse isochron ages of the three experiments gave large ranges of 2.25-3.23 and
 281 3.68-4.14 Ma, respectively, and none of these high temperature heating steps produced a statistical plateau (all MSWD > 2.0).
 282 The amount of radiogenic ^{40}Ar of both the $^{40}\text{Ar}/^{39}\text{Ar}$ result from our sample and the K-Ar age data from previous studies
 283 (Fytikas et al., 1986) is rather low ($<15\%$) for a sample of this age based on our laboratory experience. Therefore, the estimated
 284 age range for the oldest volcanic products of the Milos VF should be confirmed by other dating techniques.



285
 286 **Figure 6. Groundmass $^{40}\text{Ar}/^{39}\text{Ar}$ plateau or inverse isochron ages for samples G15M0017 (A), G15M0015 (B) and G15M0029 (C).**
 287 **Individual steps and final age calculation are reported with 1σ errors. The Profitis Ilias volcano (A, B) and dacitic Korakia dome**
 288 **(C) are located in the south-western and north-eastern parts of Milos VF, respectively (Fig. 2). See the individual steps of sample**
 289 **G15M0015 and G15M0029 in supplementary material II.**

290 Sample G15M0015 is also a cryptodome breccia from Profitis Ilias (Figure 2). Two replicate incremental step heating
 291 experiments were performed on the groundmass of this sample (VU108-Z9a and VU108-Z9b_1, Figure 6B). Experiment
 292 VU108-Z9a groundmass shows a disturbing age spectrum and ages increase from ~ 3 Ma in the initial heating steps to ~ 3.2

293 Ma, followed by a decrease to ~3 Ma in the high temperature heating steps. The consecutive heating steps only exist at the
 294 lower temperature steps yielding a “plateau” of 3.12 ± 0.02 Ma (MSWD 9.07). Due to the excess argon ($^{40}\text{Ar}/^{36}\text{Ar}$ $304.19 \pm$
 295 1.25 comprising 43.07% of the released $^{39}\text{Ar}_K$), the inverse isochron of 3.06 ± 0.02 Ma (MSWD 0.01) is more reliable for this
 296 analysis. The inverse isochron age of the second groundmass (VU108-Z9b_1) is identical at 3.04 ± 0.02 Ma (MSWD 1.14;
 297 $^{39}\text{Ar}_K$ 27.00%) and $^{40}\text{Ar}/^{36}\text{Ar}$ of 293.83 ± 1.38 obtained at high temperature steps. The two experiments are remarkably similar.
 298 Although the sample does not formally fulfil the definition of a plateau age comprising >50% $^{39}\text{Ar}_K$ released, a combined age
 299 of 3.06 ± 0.02 Ma (MSWD 1.14; $^{39}\text{Ar}_K$ 22.79%, $^{40}\text{Ar}^*$ 41.77%) most likely represents the eruption age. This $^{40}\text{Ar}/^{36}\text{Ar}$ age is
 300 consistent with the K-Ar age from the same lithology of 3.08 ± 0.08 Ma (Fytikas et al. 1986).
 301 Sample G15M0029 is an andesite collected from Korakia in the northeast of Milos (Figure 2). Two incremental heating
 302 experiments (VU108-Z16a and VU108-Z16b_1, Figure 6C) were performed on this sample. The two experiments are
 303 remarkably similar and show a decreasing age from ~2.85 Ma at the lower temperature heating steps to 2.65 Ma at the higher
 304 temperatures. The higher temperature heating steps of both experiments yielded weighted mean plateau ages of 2.67 ± 0.01
 305 Ma (MSWD 0.96; $^{39}\text{Ar}_K$ 23.61%, $^{40}\text{Ar}^*$ 56.34%; inverse isochron age 2.68 ± 0.02 Ma) and 2.69 ± 0.01 Ma (MSWD 1.32;
 306 $^{39}\text{Ar}_K$ 27.08%, $^{40}\text{Ar}^*$ 55.78%; inverse isochron age 2.67 ± 0.03 Ma). The isochron intercepts for both experiments are
 307 atmospheric. The combined age of 2.68 ± 0.01 Ma should be considered with caution due to the rather low amount of released
 308 ^{39}Ar (23-28%).



309
 310 **Figure 7. Biotite $^{40}\text{Ar}/^{39}\text{Ar}$ total fusion ages for samples G15M0006 (A) and G15M0025-26(B, C), G15M0022-24 (D-F), G15M0013**
 311 **(G) and G15M0033-35 (H-J). Data outside the shaded area are not included in the weighted mean. Individual steps and final age**
 312 **calculation are reported with 1σ errors. The Kalogeros cryptodome and Mavros Kavos lava dome are located in the north-eastern**
 313 **and south-western parts of Milos VF, respectively, and Triades lava dome, Halepa lava dome, Trachilias complex and the Kalamos**
 314 **lava are situated in the southern, northern and south-eastern parts of Milos VF, respectively (see Fig. 2).**

315 3.1.3 Single biotite grain $^{40}\text{Ar}/^{39}\text{Ar}$ fusion and/or isochron ages

316 Results of nine single fusion experiments are given in Figure 7. Nine or ten replicate single fusion experiments were conducted
 317 on 5-10 grains biotite per fusion. Sample G15M0006 is from dacite with columnar joints from the Kalogeros cryptodome in
 318 the northeast of Milos (VU108-Z11, Figure 7A). The sample shows a weighted mean age of 2.72 ± 0.01 Ma for 9 out of 10
 319 total fusion experiments (MSWD 1.95; 9/10) with an average 47.9% of radiogenic ^{40}Ar . The inverse isochron age is $2.62 \pm$

0.04 Ma (MSWD 0.99). Note that excess argon ($^{40}\text{Ar}/^{36}\text{Ar}$ 310.2 \pm 4.0) is present. Hence the inverse isochron age is younger compared to the weighted mean age. The isochron age of 2.62 \pm 0.04 Ma is considered as the best estimate for the emplacement age.

Sample G15M0025 was collected from the Mavros Kavos lava dome located in the west of Milos (Figure 2). The biotite of this sample (VU108-Z2, Figure 7B) shows a weighted mean age of 2.36 \pm 0.01 Ma (MSWD 0.70; 9/10; $^{40}\text{Ar}^*$ 37.60%, inverse isochron age 2.34 \pm 0.04 Ma) with an $^{40}\text{Ar}/^{36}\text{Ar}$ intercept of 300.6 \pm 3.5. The age of 2.36 \pm 0.01 Ma is considered the best eruption age estimate for this sample.

Sample G15M0023 and G15M0024 are from the Triades lava dome northeast of Milos (Figure 2). A mafic enclave G15M0022 (host rock G15M0021) was collected from a lava near Cape Vani (Figure 2). The total fusion experiments of the biotites show that their initial $^{40}\text{Ar}/^{36}\text{Ar}$ estimates overlap with air (296-300). The total fusion ages gave the best estimates for their eruption ages of 2.10-2.13 Ma using 22 out of 31 fusions with a range of radiogenic ^{40}Ar between 30-36% (Figure 7B).

Sample G15M0013 is from the rhyolitic Halepa lava dome in the south of Milos (Figure 2). The total fusion experiment (VU108-Z13, Figure 7C) on biotite of this sample produced a weighted mean age of 1.04 \pm 0.01 Ma (MSWD 1.62; 9/10, $^{40}\text{Ar}^*$ 26.3%; inverse isochron age 1.02 \pm 0.04 Ma) with an initial $^{40}\text{Ar}/^{36}\text{Ar}$ estimate of 299.8 \pm 4.1. The best estimate for the eruption age of the Halepa rhyolite is 1.04 \pm 0.01 Ma.

Sample G15M0034 and G15M0035 were collected from a lava dome located southeast of the Trachilas cone (Figure 2). Nine total fusion experiments (VU108-Z21, Figure 7C) were performed on biotite of sample G15M0035 and yielded the age of 0.63 \pm 0.02 Ma (MSWD 1.26; 6/9; $^{40}\text{Ar}^*$ 4.9%; inverse isochron age 0.77 \pm 0.13 Ma). The atmospheric isochron intercept overlaps with air at 2-sigma (296.4 \pm 1.7). The 4.9% of radiogenic ^{40}Ar is so low that we should consider the age of 0.63 \pm 0.02 Ma with caution. For biotite of sample G15M0034 (VU108-Z20, Figure 7C) one total fusion experiment produced a weighted mean age of 0.51 \pm 0.02 Ma (MSWD 0.95; 6/10; $^{40}\text{Ar}^*$ 3.5%; inverse isochron age 0.61 \pm 0.08 Ma) with an atmospheric isochron intercept. The age of 0.51 \pm 0.02 Ma also needs to be considered as possibly suspect due to the low amount of radiogenic ^{40}Ar .

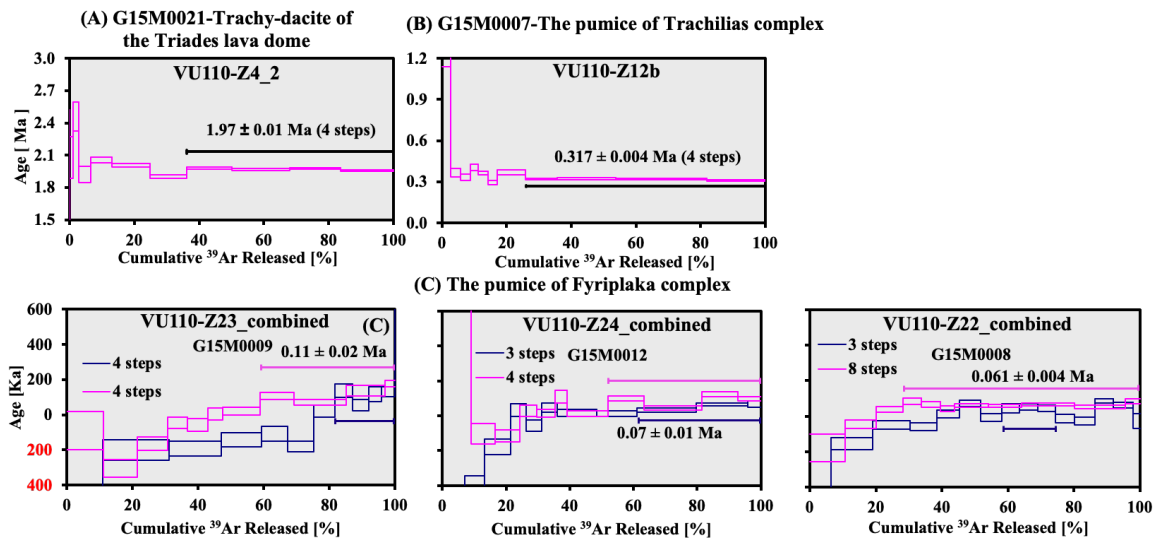


Figure 8. Biotite $^{40}\text{Ar}/^{39}\text{Ar}$ plateau ages for samples G15M0021 (A), G15M0007 (B), and G15M0009 (VU110-Z23_combined), G15M0012 (VU110-Z24_combined) and G15M0008 (VU110-Z22_combined) (C). The numbers in red represent negative ages. Individual steps and final age calculation are reported with 1 σ errors. The Triades lava dome, Trachilias and Fyriplaka complexes are located in the north-western, northern and south-eastern parts of Milos VF, respectively (see Fig. 2). See the individual steps of sample G15M0021, G15M0007, G15M0009, G15M0012 and G15M0008 in supplementary material II.

Sample G15M0033 was collected from the Kalamos lava along the coast of the southwest of the Fyriplaka rhyolitic complex (Figure 2). Biotite of this sample (VU108-Z19, Figure 7C) yielded 0.412 \pm 0.004 Ma (MSWD 1.10; 8/10; inverse isochron age 0.39 \pm 0.02 Ma) with \sim 22.2% of radiogenic ^{40}Ar which is considered as the eruption age for the Kalamos lava.

352 3.1.4 Multiple biotite grain $^{40}\text{Ar}/^{39}\text{Ar}$ incremental heating plateau and/or isochron ages

353 Figure 8 displays the biotite $^{40}\text{Ar}/^{39}\text{Ar}$ ages measured by the incremental heating steps method. Sample G15M0021 is the host
354 lava of mafic enclave G15M0022. Twelve replicate total fusion experiments on its biotite (VU110-Z4, Table 3) produced an
355 age of 2.48 ± 0.04 Ma (MSWD 1.49; 4/12, $^{40}\text{Ar}^*$ 36.09%; inverse isochron age 3.44 ± 0.46 Ma). Although this suggests a
356 correct age, the large analytical error of each fusion (>0.3 Ma on average) and poor reproducibility (4/12) of this experiment
357 probably results in an unreliable age. Therefore, two more incremental heating experiments were performed on this sample
358 (VU110-Z4_2 and VU110-Z4_2b, Figure 8A), that gave an age of 1.97 ± 0.01 Ma (MSWD 1.66; $^{39}\text{Ar}_K$ 63.8%, $^{40}\text{Ar}^*$ 54.7%;
359 inverse isochron age 1.97 ± 0.03 Ma) and 2.01 ± 0.01 Ma (MSWD 6.76; $^{39}\text{Ar}_K$ 75.39%, $^{40}\text{Ar}^*$ 57.84%; inverse isochron age
360 2.04 ± 0.05 Ma), respectively. The scatter in the latter is too high to define a reliable plateau age and the first incremental
361 heating experiment is considered as the best estimate of the eruption age of this sample.

362 Sample G15M0007 was collected from the rhyolitic Trachilas complex in the north of Milos (Figure 2). Twenty-two total
363 fusion (VU110-Z12, Table 3) and two incremental heating experiments (VU110-Z12a and 12b, Figure 8B) were performed
364 on biotite of this sample. The total fusion experiments did not result in a reliable age due to the large errors of single steps (\pm
365 0.19 Ma on average) and the rather low amount of radiogenic ^{40}Ar (9.1%). On the other hand, the first incremental heating
366 experiment produced a plateau age of 0.30 ± 0.01 Ma (MSWD 4.61; $^{39}\text{Ar}_K$ 56.60%; inverse isochron age 0.28 ± 0.05 Ma)
367 including 14.51% of radiogenic ^{40}Ar . The second incremental heating experiment yielded a plateau of 0.317 ± 0.004 Ma
368 (MSWD 1.29; $^{39}\text{Ar}_K$ 74.05%; inverse isochron age 0.31 ± 0.03 Ma) with a higher amount of radiogenic ^{40}Ar (18.30%). The
369 isochron intercepts of both incremental heating experiments are atmospheric. The second experiment is the best estimate for
370 the eruption age, since it contained the largest amount of radiogenic ^{40}Ar and has a better reproducibility of single heating
371 steps.

372 Three pumice clasts (G15M0008-9 and G15M0012) were sampled from different layers of the Fyriplaka complex (Figure 2).
373 The first incremental step heating experiment on biotite from sample G15M0009 (VU110-Z23a, Figure 8C) gave negative
374 ages at the lower temperature heating steps. Four consecutive higher temperature heating steps seem to define a “plateau” of
375 0.11 ± 0.02 Ma (MSWD 1.37) only using 18.33% of the total $^{39}\text{Ar}_K$ with 1.65% of radiogenic ^{40}Ar . The second experiment
376 (VU110-Z23b) also yielded a “plateau” of 0.11 ± 0.03 Ma (MSWD 6.77) at higher temperature heating steps including 41.05%
377 of the total $^{39}\text{Ar}_K$ and 3.13% of radiogenic ^{40}Ar . The significantly larger error of the isochron age may be due to the clustering
378 of data close to zero on the y-axis. The two experiments (VU110-Z23a and Z23b) are comparable. The combined age of 0.11
379 ± 0.02 (MSWD 3.5) is consistent with the age of 0.09-0.14 Ma from Fytikas et al. (1986). Although only 29.50% of the released
380 $^{39}\text{Ar}_K$ was used for this sample, we believe this age is the eruption age of this layer in the Fyriplaka complex.

381 For biotite of sample G15M0012, both incremental step heating experiments are comparable. Both of them yielded plateau
382 ages of 0.05 ± 0.01 Ma (VU110-Z24a; MSWD 3.09; $^{39}\text{Ar}_K$ 38.89%, $^{40}\text{Ar}^*$ 2.89%; inverse isochron age 0.14 ± 0.03 Ma) and
383 0.09 ± 0.02 Ma (VU110-Z24b; MSWD 8.16; $^{39}\text{Ar}_K$ 48.04%, $^{40}\text{Ar}^*$ 4.59%; inverse isochron age 0.09 ± 0.05 Ma) at higher
384 temperature heating steps (Figure 8C). The clustering of data points of experiment VU110-Z24a could result in the lower
385 initial estimate of $^{40}\text{Ar}/^{36}\text{Ar}$ (285.98 ± 4.76). However, the combined age of 0.07 ± 0.01 Ma, using 43.53% of the total $^{39}\text{Ar}_K$
386 with an atmospheric isochron intercept (295.67 ± 7.39), could be the representative age of eruption.

387 Biotite of sample G15M0008 did not result in a reliable plateau in the first incremental step heating experiment (VU110-Z22a,
388 Figure 8C) but shows a very disturbed age spectrum. The second experiment (VU110-Z22b) yielded 0.062 ± 0.003 Ma (MSWD
389 0.91) using 71.81% of the total $^{39}\text{Ar}_K$ with 2.69% of radiogenic ^{40}Ar as the best estimate of the eruption age.

390 3.1.5 Multiple amphibole grain $^{40}\text{Ar}/^{39}\text{Ar}$ multi-grain incremental heating plateau and/or isochron ages

391 There are only two amphibole samples that yielded $^{40}\text{Ar}/^{36}\text{Ar}$ plateau and/or isochron ages (Figure 9A and B). Sample
392 G15M0004 was collected from the pyroclastic series of Adamas from the PSLD (Fytikas et al., 1986), to the north of Bombarda
393 (Figure 2). Two replicate heating experiments of G15M0004 amphibole (VU108-Z10_1 and VU108-Z10_2) were performed

394 Table 2. Incremental heating ⁴⁰Ar/³⁹Ar results of the Milos volcanic field.

Volcanic Unit	Sample -ID	Irr-ID	Latitude	Age ± 1σ (Ma)	MS WD	³⁹ Ar _K (%)	n/ntotal	⁴⁰ Ar* (%)	K/Ca ± 1σ	Inverse isochron age (Ma)	⁴⁰ Ar/ ³⁶ Ar ± 1σ	MS WD
Fyriplaka Complex	G15 M00 08 ^B	VU110-Z22a	36.67 29 N	0.05 ± 0.01	0.04	16.24	3/15	1.20	60.9 ± 10.6	0.05 ± 0.10	298.08 ± 8.77	0.08
		VU110-Z22b	24.46 70 E	0.062 ± 0.003	0.91	71.81	8/11	2.69	57.3 ± 8.4	0.06 ± 0.02	299.39 ± 3.66	1.09
		Combined (Z22)	70 E	0.061 ± 0.004	0.82	41.37	11/26	2.29	58.0 ± 6.3	0.07 ± 0.01	296.78 ± 1.78	0.83
	G15 M00 12 ^B	VU110-Z24a	36.67 95 N	0.05 ± 0.01	3.09	38.89	3/11	2.89	40.0 ± 6.0	0.14 ± 0.03	285.98 ± 4.76	0.07
		VU110-Z24b	24.48 28 E	0.09 ± 0.02	8.16	48.04	4/11	4.59	30.1 ± 7.1	0.09 ± 0.05	297.46 ± 10.29	12.78
		Combined(Z24)	28 E	0.07 ± 0.01	7.44	43.53	7/22	3.86	32.3 ± 5.0	0.09 ± 0.03	295.67 ± 7.39	9.02
	G15 M00 09 ^B	VU110-Z23a	36.67 16 N	0.11 ± 0.02	1.37	18.33	4/12	1.65	45.4 ± 7.3	0.76 ± 0.30	268.52 ± 17.08	0.90
VU110-Z23b		24.48 91 E	0.11 ± 0.03	6.77	41.05	4/11	3.13	19.4 ± 3.7	0.29 ± 0.14	285.17 ± 15.80	8.09	
Combined (Z23)		91 E	0.11 ± 0.02	3.50	29.50	8/21	2.39	19.7 ± 2.6	0.15 ± 0.05	295.78 ± 4.34	4.04	
Trachilas Complex	G15 M00 07 ^B	VU110-Z12a	36.76 71 N	0.30 ± 0.01	4.61	56.50	8/16	14.51	38.3 ± 2.4	0.28 ± 0.05	301.42 ± 9.01	5.47
		VU110-Z12b	24.41 24 E	0.317 ± 0.004	1.29	74.05	4/11	18.30	32.0 ± 2.5	0.31 ± 0.03	299.52 ± 6.40	2.04
		Combined (Z12)	24 E	0.31 ± 0.01	5.57	65.27	12/27	15.77	33.1 ± 1.6	0.34 ± 0.03	293.05 ± 5.50	5.84
Kontaro dome	G15 M00 20 ^G	VU108-Z5a_5	36.72 34 N	1.52 ± 0.01	1.06	61.82	8/12	18.30	1.51 ± 0.05	1.49 ± 0.02	300.03 ± 0.86	0.95
		VU108-Z5b_1	24.39 52 E	1.56 ± 0.01	1.94	41.54	3/10	47.94	1.73 ± 0.06	1.58 ± 0.02	294.97 ± 3.74	2.17
		VU108-Z5b_2	24.39 52 E	1.52 ± 0.01	1.73	62.45	5/10	22.95	1.56 ± 0.08	1.53 ± 0.02	298.12 ± 0.89	2.34
		Combined (Z5)	52 E	1.54 ± 0.01	3.06	57.32	16/32	25.31	1.58 ± 0.04	1.55 ± 0.01	297.41 ± 0.57	2.82
	G15 M00 19 ^G	VU108-Z6a_4	36.72 11 N	1.62 ± 0.01	3.80	89.75	9/11	34.28	0.91 ± 0.05	1.62 ± 0.02	297.66 ± 1.36	4.40
		VU108-Z6a_5	24.39 50 E	1.55 ± 0.01	4.50	95.41	10/12	35.26	0.88 ± 0.06	1.55 ± 0.01	298.73 ± 1.29	5.40
		VU108-Z6b_1	24.39 50 E	1.56 ± 0.01	4.05	56.64	4/10	53.19	1.02 ± 0.01	1.48 ± 0.02	315.46 ± 5.20	0.44
Combined (Z6)	50 E	1.55 ± 0.01	32.15	80.97	27/45	38.78	0.93 ± 0.04	1.53 ± 0.02	300.60 ± 2.27	34.25		
Dheme-neghaki volcano	G15 M00 32B ^O	VU108-Z18	36.70 84 N 24.53 24 E	1.825 ± 0.002	0.91	98.64	12/13	93.86	1.83 ± 0.04	1.825± 0.003	301.52 ± 3.34	0.93
Triades lava dome	G15 M00 21 ^B	VU110-Z4_2	36.74 02 N	1.97 ± 0.01	1.66	63.83	4/12	54.72	107.55 ± 20.64	1.97 ± 0.03	299.16 ± 5.36	2.56
		VU110-Z4_2b	24.33 97 E	2.01 ± 0.01	6.76	75.39	6/16	57.84	54.43 ± 8.29	2.04 ± 0.05	293.08 ± 10.44	8.15
		Combined (Z4)	97 E	1.99 ± 0.01	9.08	69.12	10/28	56.59	73.52 ± 6.46	2.00 ± 0.04	295.64 ± 7.89	10.30
Adamas lava dome	G15 M00 04 ^A	VU108-Z10_1	36.72 82 N	2.99 ± 0.11	1.00	87.31	4/12	16.36	0.030 ± 0.002	7.89 ± 2.46	202.39 ± 48.47	0.01
		VU108-Z10_2	24.43 15 E	2.86 ± 0.09	1.50	86.18	7/11	17.58	0.029 ± 0.002	0.70 ± 0.29	348.91 ± 27.33	1.00
		Combined (Z10)	15 E	2.90 ± 0.07	1.31	86.74	11/23	17.13	0.029 ± 0.001	1.95 ± 0.45	319.51 ± 14.70	1.17
The dyke of Mavro Vouni lava dome	G15 M00 16 ^G	VU108-Z8a	36.66 68 N	2.71 ± 0.02	2.31	79.64	8/12	16.57	0.24 ± 0.05	2.65 ± 0.10	299.84 ± 2.32	2.92
		VU108-Z8a_4	24.33 98 E	2.61 ± 0.03	0.93	57.41	7/12	16.86	0.12 ± 0.07	2.69 ± 0.10	296.44 ± 2.49	0.69
		VU108-Z8b_1	24.33 98 E	2.67 ± 0.01	1.50	65.57	7/11	17.25	0.11 ± 0.04	2.55 ± 0.05	301.53 ± 1.14	0.71
		Combined (Z8)	98 E	2.66 ± 0.01	2.51	67.27	22/35	16.87	0.14 ± 0.02	2.61 ± 0.05	300.01 ± 1.18	2.78
Korokia dome	G15 M00 29 ^G	VU108-Z16a	36.74 65 N	2.67 ± 0.01	0.96	23.61	4/13	56.34	0.53 ± 0.05	2.68 ± 0.02	296.64 ± 3.18	1.25
		VU108-Z16b_1	24.52 00 E	2.69 ± 0.01	1.32	27.08	3/13	55.78	0.55 ± 0.04	2.67 ± 0.03	301.16 ± 4.72	2.13
		Combined (Z16)	00 E	2.68 ± 0.01	1.66	25.30	7/26	56.10	0.54 ± 0.03	2.67 ± 0.02	300.00 ± 2.94	1.98
Coherent dacite of Profitis Illias volcano	G15 M00 15 ^G	VU108-Z9a	36.66 29 N	3.12 ± 0.02	9.07	43.07	3/12	42.73	1.31 ± 0.05	3.06 ± 0.02	304.19 ± 1.25	0.01
		VU108-Z9b_1	24.35 96 E	2.98 ± 0.02	4.53	27.00	4/14	39.35	0.98 ± 0.06	3.04 ± 0.02	293.83 ± 1.38	1.14
		Combined (Z9)	96 E	2.99 ± 0.02	5.54	22.79	6/26	41.77	1.00 ± 0.04	3.06 ± 0.02	292.77 ± 1.62	1.90
Coherent dacite of Profitis Illias volcano	G15 M00 17 ^G	VU108-Z7a	36.65 96 N	3.64 ± 0.08	3.13	28.62	7/13	9.77	1.04 ± 0.02	4.14 ± 0.49	293.87 ± 4.77	3.44
		VU108-Z7a_4	24.36 75 E	4.10 ± 0.06	2.13	34.71	6/17	9.08	1.10 ± 0.01	4.11 ± 1.40	298.44 ± 15.51	3.24
		VU108-Z7b_1	24.36 75 E	3.41 ± 0.05	3.95	31.41	5/13	9.95	1.00 ± 0.03	3.68 ± 0.71	295.97 ± 7.34	7.09
		Combined (Z7)	75 E	3.63 ± 0.08	14.04	31.40	18/43	9.59	1.04 ± 0.02	2.19 ± 0.32	311.31 ± 3.60	10.19

395 The age in bold is considered as the best estimate of the eruptive age.
 396 The ⁴⁰Ar* (%) is the average radiogenic ⁴⁰Ar of the analyses included in the weighted mean.
 397 The experiment was analyzed on biotite^B, obsidian^O, amphibole^A and groundmass^G of a sample.
 398 The same steps were used for the calculation of isochron ages as used in the weighted mean ages.

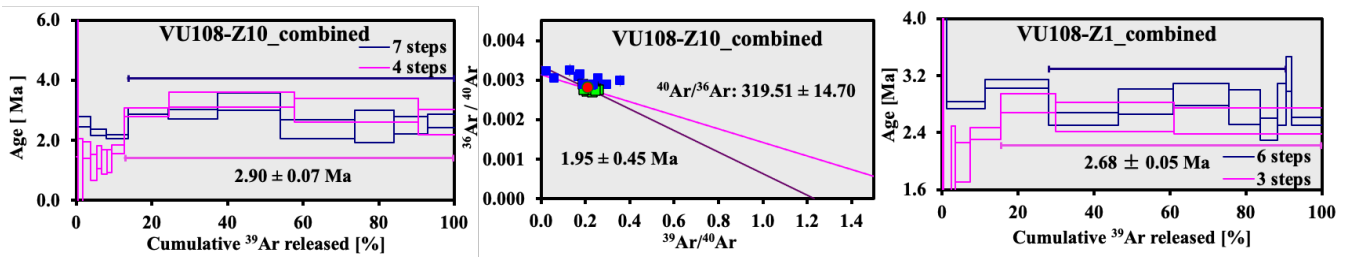
399 **Table 3.** $^{40}\text{Ar}/^{39}\text{Ar}$ results of single grain fusion analyses on the Milos volcanic field.

Volcanic unit	Sample-ID	Irr-ID	Location	Age $\pm 1\sigma$ (Ma)	MS WD	$^{39}\text{Ar}_K$ (%)	n/ntotal	$^{40}\text{Ar}^*$ (%)	K/Ca $\pm 1\sigma$	Inverse isochron age (Ma)	$^{40}\text{Ar}/^{36}\text{Ar} \pm 1\sigma$	MS WD
Fyriplaka complex	G15M0008 ^B	VU11 0-Z22	36.6729 N 24.4670 E	0.71 \pm 0.06	0.41	25.78	8/23	8.67	17.5 \pm 1.8	0.64 \pm 0.20	302.75 \pm 12.62	0.46
	G15M0012 ^B	VU11 0-Z24	36.6795 N 24.4828 E	1.12 \pm 0.11	2.26	60.49	14/23	7.32	14.9 \pm 0.8	0.26 \pm 0.07	316.75 \pm 19.49	2.29
	G15M0009 ^B	VU11 0-Z23	36.6716 N 24.4891 E	0.65 \pm 0.07	1.16	79.91	19/23	5.87	12.0 \pm 0.5	0.28 \pm 0.07	309.57 \pm 16.01	1.22
Trachilas complex	G15M0007 ^B	VU11 0-Z12	36.7671 N 24.4124 E	0.47 \pm 0.05	0.75	72.65	15/22	9.09	14.8 \pm 0.5	0.55 \pm 0.12	293.95 \pm 11.30	0.80
Kalamos lava	G15M0033 ^B	VU10 8-Z19	36.6662 N 24.4652 E	0.412 \pm 0.004	1.10	77.24	8/10	22.22	20.5 \pm 2.7	0.39 \pm 0.02	303.32 \pm 3.06	0.89
Trachilas complex	G15M0034 ^B	VU10 8-Z20	36.7550 N 24.4244 E	0.51 \pm 0.02	0.95	56.92	6/10	3.53	13.7 \pm 1.2	0.61 \pm 0.08	296.45 \pm 1.65	0.92
	G15M0035 ^B	VU10 8-Z21	36.7550 N 24.4244 E	0.63 \pm 0.02	1.26	73.43	6/9	4.87	17.7 \pm 1.1	0.77 \pm 0.13	294.99 \pm 3.17	1.42
Halepa lava dome	G15M0013 ^B	VU10 8-Z13	36.6716 N 24.4406 E	1.04 \pm 0.01	1.62	82.40	9/10	26.30	*15.2 \pm 0.2	1.02 \pm 0.04	299.77 \pm 4.06	0.00
Triades lava dome	G15M0021 ^B	VU11 0-Z4	36.7402 N 24.3397 E	2.48 \pm 0.04	1.49	87.08	4/12	36.09	13.00 \pm 0.60	3.44 \pm 0.46	228.58 \pm 36.66	1.39
	G15M0022 ^B	VU10 8-Z14	36.7402 N 24.3397 E	2.10 \pm 0.01	1.37	100.0 0	10/10	36.04	*11.7 \pm 0.2	2.08 \pm 0.06	299.44 \pm 4.63	1.59
	G15M0023 ^B	VU10 8-Z3	36.7263 N 24.3420 E	2.10 \pm 0.01	1.72	55.58	6/11	35.93	*76.1 \pm 2.4	2.13 \pm 0.06	296.12 \pm 4.63	2.08
	G15M0024 ^B	VU10 8-Z15	36.7277 N 24.3415 E	2.13 \pm 0.01	0.46	63.67	6/10	29.74	22.5 \pm 3.2	2.09 \pm 0.03	300.50 \pm 1.58	0.23
Mavros Kavos lava dome	G15M0025 ^B	VU10 8-Z2	36.6876 N 24.3515 E	2.36 \pm 0.01	0.70	84.62	9/10	37.62	43.2 \pm 2.7	2.34 \pm 0.04	300.57 \pm 3.49	0.78
	G15M0026 ^B	VU10 8-Z1b	36.6848 N 24.3500 E	2.35 \pm 0.01	1.36	95.23	9/10	38.56	12.8 \pm 2.3	2.42 \pm 0.04	292.01 \pm 2.92	0.93
Kalegero scrypto-dome	G15M0006 ^B	VU10 8-Z11	36.7643 N 24.5157 E	2.72 \pm 0.01	1.95	87.67	9/10	47.90	*28.3 \pm 0.5	2.62 \pm 0.04	310.21 \pm 4.04	0.99

400 The age in bold is considered as the best estimate of the eruptive age.
 401 The $^{40}\text{Ar}^*$ (%) is the average radiogenic ^{40}Ar of the analyses included in the weighted mean.
 402 *The K/Ca ratio is calibrated by removing the total fusion with excess ^{37}Ar (Ca) ($f_A > 1$).
 403 ^BThe experiment was analyzed on biotite of the sample.
 404 The same steps were used for the calculation of isochron ages as used in the weighted mean ages.

(A) G15M0004-The dacite of Adamas lava dome

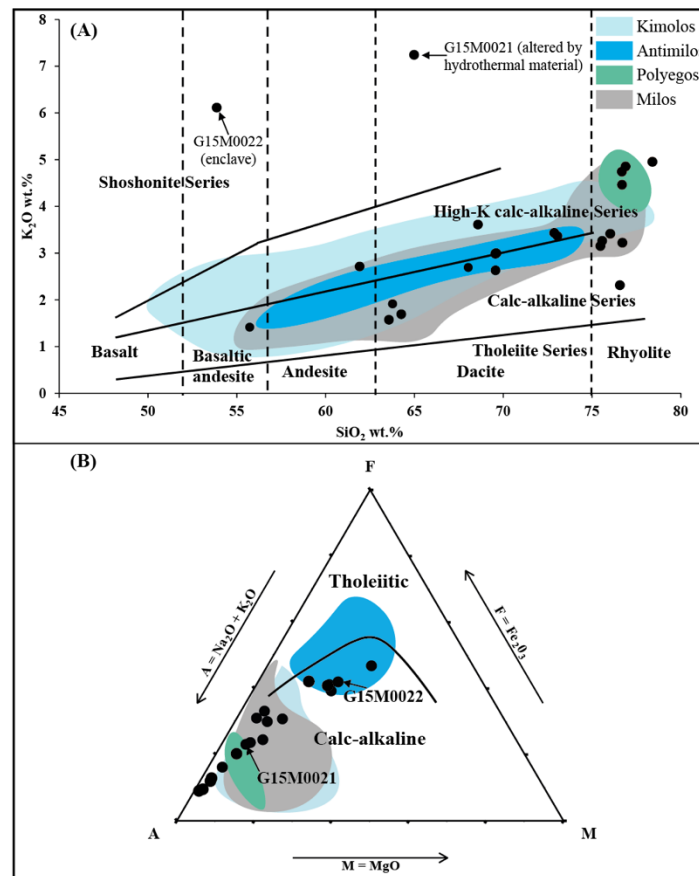
(B) G15M0026-The dacite of Mavros Kavos lava dome



405 **Figure 9.** Amphibole $^{40}\text{Ar}/^{39}\text{Ar}$ plateau or inverse isochron ages for samples G15M0004 (A) and G15M0026 (B). Final age
 406 calculation is reported with 1σ errors. The Adamas and Mavros Kavos lava domes are located in the northern and south-western
 407 parts of Milos VF, respectively (see Fig. 2). See the individual steps of sample G15M0004 and G15M0026 in supplementary
 408 material II.
 409

410 yielding 2.99 ± 0.11 Ma (MSWD 1.00; $^{39}\text{Ar}_K$ 87.31%, $^{40}\text{Ar}^*$ 16.36%; inverse isochron age 7.89 ± 2.46 Ma) and 2.86 ± 0.09
 411 Ma (MSWD 1.50; $^{39}\text{Ar}_K$ 86.18%, $^{40}\text{Ar}^*$ 17.58%; inverse isochron age 0.70 ± 0.29 Ma). The variable atmospheric isochron
 412 intercept of both experiments ($^{40}\text{Ar}/^{36}\text{Ar}$ 202.39 ± 48.47 and 348.91 ± 27.33) is due to the clustering of the data points. Note
 413 that also the amount of radiogenic ^{40}Ar is rather low ($\sim 17\%$). The two experiments are remarkably similar. A combined inverse

414 isochron age of 1.95 ± 0.45 Ma (MSWD 1.17; $^{40}\text{Ar}/^{36}\text{Ar}$ 319.51 \pm 14.70) is considered the best estimate, but ideally this age
 415 should be checked by other techniques.
 416 Sample G15M0026 is from the same location as sample G15M0025, which gives us the opportunity to compare the biotite age
 417 with the amphibole age. One total fusion experiment on biotite (VU108-Z1b) yielded a weighted mean age of 2.35 ± 0.01 Ma
 418 (MSWD 1.36; $^{40}\text{Ar}^*$ 38.6%). The atmospheric isochron intercept is low ($^{40}\text{Ar}/^{36}\text{Ar}$ 292.01 \pm 2.92), the inverse isochron age of
 419 2.42 ± 0.04 Ma (MSWD 0.93) is considered the best result from the biotite. Two incremental heating experiments for
 420 amphibole (VU108-Z1b_1 and VU108-Z1b_2) gave plateau ages of 2.67-2.70 Ma which are much higher values than the
 421 biotite inverse isochron ages (2.28-2.31 Ma). This result could be caused by the high $^{40}\text{Ar}/^{36}\text{Ar}$ isochron intercepts (>320) with
 422 large uncertainties of ~ 29 . Therefore, on the basis of the remarkable similarity of the two experiments, the combined inverse
 423 isochron age of 2.31 ± 0.28 Ma (MSWD 0.93, $^{39}\text{Ar}_K$ 71.36%, $^{40}\text{Ar}^*$ 34.97%) is considered as the best estimate from amphibole
 424 which overlaps with the biotite age of 2.42 ± 0.03 Ma. This biotite age of 2.42 ± 0.03 Ma is considered to the best approximation
 425 of the eruption age.



426
 427 **Figure 10. SiO₂ versus K₂O (A) and AFM (B) diagrams for the Milos volcanic field with data of this study as solid circles.**
 428 **Published data are represented by shaded fields (Francalanci and Zelmer, 2019 and reference therein). Fields for the tholeiitic,**
 429 **calc-alkaline, high-K calc-alkaline and shoshonitic series are from Peccerillo and Taylor (1976). Vertical lines defining fields for**
 430 **basalt, basaltic-andesite, andesite, dacite and rhyolite are from Le Bas et al. (1986). The solid line dividing tholeiitic and calc-**
 431 **alkaline fields is from Irvine and Baragar (1971).**

432 3.2 Major element results

433 Major-element results are given in Table 4. The major element compositions range from 54 to 78 wt.% SiO₂ (basaltic-andesite-
 434 rhyolite to dacite-rhyolite, see Figure 10A). The most felsic samples (SiO₂>75 wt.%) belong to the Fyriplaka and Trachilas
 435 complexes. Our data overlap with those of previous studies and display a similar range in SiO₂-K₂O (Francalanci and Zellmer,
 436 2019 and reference therein). The samples of Polyegos are similar to the Fyriplaka and Trachilas complexes, whereas the older
 437 Milos samples overlap with Kimolos and Antimilos (Fytikas et al., 1986, Francalanci et al., 2007).
 438 Although some samples of Antimilos are tholeiitic, all of the Milos volcanic units belong to the calc-alkaline and medium to
 439 high-K series (Figure 10B). A mafic inclusion, sample G15M0022, has high K₂O (6%), similar to sample G15M0021 (7.2

440 wt.%). Both of them were collected from the Vani Cape area (Fig. 2). The SiO₂ wt.% versus our ⁴⁰Ar/³⁹Ar ages diagram (Figure
 441 11A) shows that there is a tendency of the volcanic units to become more felsic over time. In the diagram with K₂O/SiO₂
 442 versus age there is no significant change (Figure 11C).

443 **Table 4. Major-element composition of volcanic samples from the Milos Volcanic Field.**

Sample-ID	G15M0 008	G15M0 012	G15M0 009	G15M0 007	G15M0 033	G15M0 034	G15M0 035	G15M0 013	G15M 0020	G15M 0019	G15M00 32B	G15M0 004
Rock Types	Pumice	Pumice	Pumice	Pumice	Pumice	Pumice	Pumice	Rhyolite	-	Dacite	Obsidian	Dacite
Period	III							II				
Major elements (wt.%)												
SiO ₂	76.71	75.47	76.02	76.68	76.68	76.89	78.40	72.87	-	64.26	75.57	63.56
TiO ₂	0.14	0.13	0.13	0.08	0.10	0.08	0.08	0.22	-	0.56	0.20	0.57
Al ₂ O ₃	12.96	12.77	12.91	12.60	12.86	12.64	12.93	14.11	-	16.08	13.32	16.09
Fe ₂ O ₃	1.11	1.08	1.04	0.85	0.88	0.84	0.85	1.95	-	5.33	1.46	5.70
MnO	0.06	0.06	0.06	0.08	0.09	0.09	0.09	0.07	-	0.11	0.06	0.11
MgO	0.22	0.22	0.23	0.11	0.18	0.11	0.11	0.51	-	2.42	0.33	2.81
CaO	1.27	1.27	1.19	0.75	0.85	0.74	0.76	2.23	-	5.33	1.71	6.01
Na ₂ O	4.04	4.12	3.99	3.58	3.71	3.50	3.49	3.73	-	3.60	3.95	3.49
K ₂ O	3.22	3.15	3.41	4.74	4.46	4.85	4.95	3.43	-	1.69	3.26	1.57
P ₂ O ₅	0.02	0.02	0.02	0.01	0.01	0.01	0.01	0.04	-	0.04	0.03	0.09
BaO	0.06	0.06	0.06	0.05	0.05	0.05	0.05	0.06	-	0.04	0.06	0.04
L.O.I.	0.16	0.35	0.16	0.17	0.14	0.33	0.06	0.13	-	0.09	0.07	0.04
Total	99.97	98.70	99.22	99.70	100.01	100.13	101.78	99.35	-	99.55	100.02	100.08

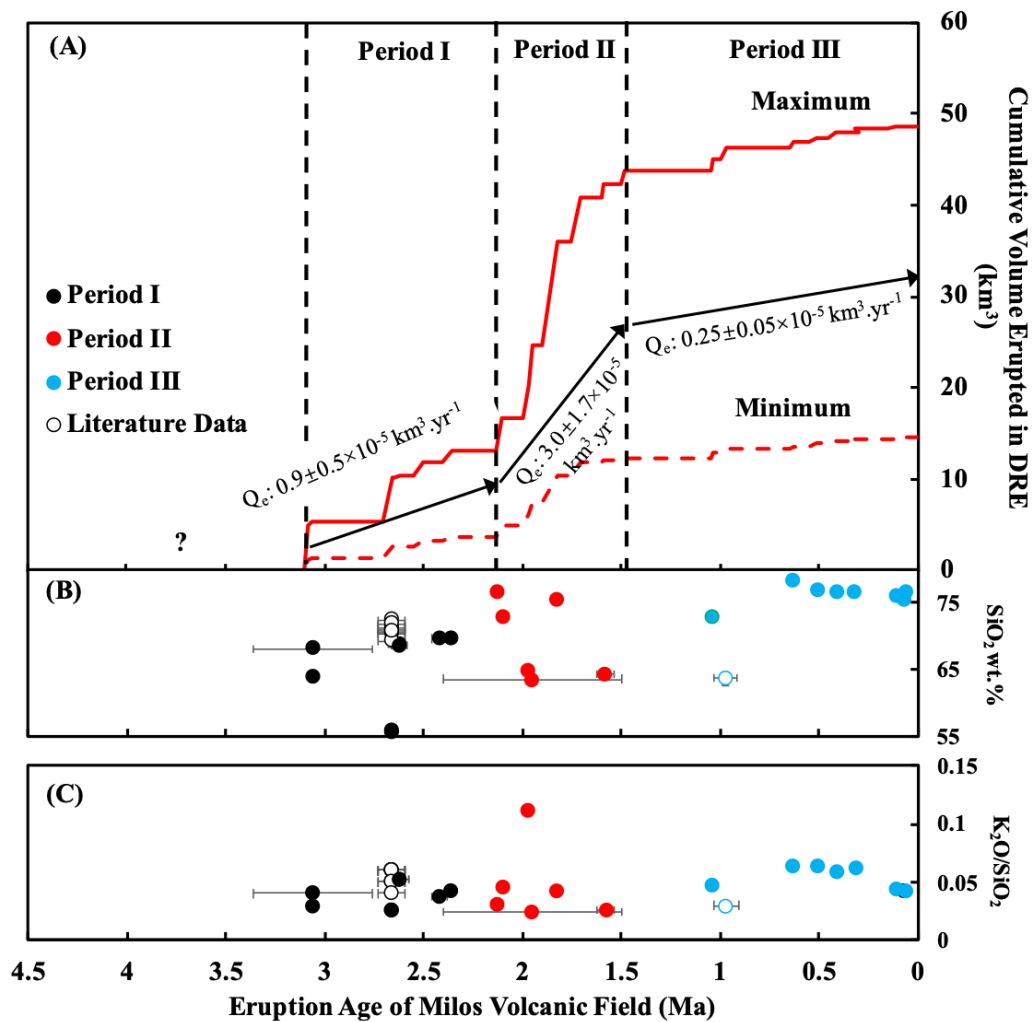
444

Sample-ID	G15M0 021	G15M0 022	G15M0 023	G15M0 024	G15M0 025	G15M0 026	G15M0 006	G15M0 016	G15M0 029	G15M0 015	G15M0 017	
Rock Types	Trachy- dacite	Enclave	Dacite	Rhyolite	Dacite	Dacite	Dacite	Basaltic Andesite	Dacite	Dacite	Dacite	
Period	II					I						
Major elements (wt.%)												
SiO ₂	64.98	53.87	73.05	76.57	69.56	69.57	68.58	55.72	61.91	63.77	68.03	
TiO ₂	0.35	0.60	0.29	0.23	0.42	0.43	0.40	0.66	0.79	0.64	0.58	
Al ₂ O ₃	16.82	19.91	14.24	11.73	15.30	16.08	15.90	18.43	17.09	16.33	15.90	
Fe ₂ O ₃	3.69	7.61	3.23	1.69	3.15	3.38	2.67	7.70	5.90	5.42	3.47	
MnO	0.08	0.16	0.02	0.03	0.11	0.04	0.07	0.14	0.09	0.10	0.07	
MgO	1.50	3.93	0.53	0.46	0.88	0.62	0.81	4.42	1.84	2.48	1.34	
CaO	2.19	5.45	2.35	2.36	3.67	3.43	2.89	8.78	6.07	5.91	4.31	
Na ₂ O	2.61	1.73	3.28	2.85	3.49	3.56	4.19	2.90	3.57	3.35	3.76	
K ₂ O	7.24	6.11	3.36	2.31	2.98	2.63	3.61	1.41	2.71	1.91	2.69	
P ₂ O ₅	0.05	0.08	0.04	0.05	0.11	0.09	0.11	0.09	0.20	0.09	0.10	
BaO	0.35	0.34	0.06	0.05	0.06	0.06	0.10	0.03	0.13	0.04	0.04	
L.O.I.	0.17	0.21	0.12	0.20	0.19	0.09	0.12	0.06	0.09	0.04	0.48	
Total	100.03	100.00	100.57	98.53	99.92	99.98	99.45	100.34	100.39	100.08	100.77	

445 The classification of rock type for each sample is on the basis of field observation and SiO₂ versus K₂O plot of Le Bas et al. (1986). All iron
 446 expressed as Fe₂O₃T(otal).

447 3.3 Variations of eruption volume with ages

448 Figure 11a shows the cumulative volcanic output volume of the Milos VF over time. This diagram shows that the Milos VF
 449 can be separated into three periods: Periods I (~3.3-2.13 Ma) and III (1.48-0.00 Ma) are characterised by low volcanic output
 450 volumes, whereas Period II (2.13-1.48 Ma) shows a rapid increase in volcanic output volume. Period I and II are build up in
 451 submarine settings, whereas Period III is in a subaerial setting. The Milos VF was largely (~85% by volume) constructed in
 452 submarine before ~1.48 Ma (Period I and II) (Figure 11A). During Period III (1.48 Ma-present), only a small volume (~15%)
 453 of rhyolitic magma was added from different eruption vents. See the details of Period I-III in section 4.3.2.



454

455

456

457

458

459

460

461

Figure 11. Eruption age versus (A) cumulative eruption volume for the volcanic deposits of Milos, (B) SiO₂ wt.%, (C) K₂O%/SiO₂%, of Milos volcanic units of this study and previous studies. The maximum (Max; red line) and minimum (Min; dashed red line) cumulative eruption volume curves were estimated from Campos et al. (1996) and Stewart and McPhie (2006). Q_e is the long-term volumetric volcanic output rate (see discussion). The exact volume of volcanic products between 4.1 and 3.08 Ma is not well constrained and indicated with a question mark. The major element data of the old pumices of Filakopi volcanoes (2.66 Ma) are from Stewart (2003). The major element data of the Plakes lava dome is from Fytikas et al. (1986). Geochemical data of the old pumices of the Profitis Ilias (~3.08 Ma) is lacking due to the severe alteration.

462

4 Discussion

463

464

465

In this section, our ⁴⁰Ar/³⁹Ar results are compared with previously published geochronological data, and subsequently used to refine the stratigraphy of the Milos VF. In the last part, we will discuss the temporal variations in major elements and the volumetric volcanic output rate of the Milos VF.

466

4.1 Comparison with the previous geochronological studies on the Milos VF

467

468

469

470

471

472

473

474

K-Ar ages may show undesirable and unresolvable scatter due to various problems: (1) inaccurate determination of radiogenic argon due to either incorporation of excess argon or incomplete degassing of argon during the experiments; (2) inclusion of cumulate or wall rock phenocrysts in bulk analyses; (3) disturbance of a variety of geological processes such as slow cooling, thermal reheating; (4) unrecognized heterogeneities due to separate measurements of potassium and argon content by different methods; (5) requirement of relatively large quantities (milligrams) of pure sample (e.g. Lee, 2015). In addition to these methodological issues, in the case of Milos we observe that hydrothermal alteration caused substantial kaolinitisation, in particular the felsic volcanic samples, that most likely has affected the K-Ar systematics. Some of these issues are also valid for the ⁴⁰Ar/³⁹Ar method. However, the K-Ar method does not allow testing if ages are compromised.

475 $^{40}\text{Ar}/^{39}\text{Ar}$ ages only need isotopes of argon to be measured from a single aliquot of sample with the same equipment that can
476 eliminate some of the problems with sample inhomogeneity. Furthermore, step heating and multiple single fusion experiments
477 can shed light on sample inhomogeneity due to partial alteration effects. The high sensitivity of modern noble gas mass
478 spectrometers for $^{40}\text{Ar}/^{39}\text{Ar}$ measurements results in very small sample amounts needed for analysis, that can yield more
479 information on the thermal or alteration histories than larger samples. Moreover, other argon isotopes (^{36}Ar , ^{37}Ar and ^{38}Ar) can
480 be used to infer some information about the chemical compositions (i.e. Ca and Cl) of samples. A high-resolution laser
481 incremental heating method of $^{40}\text{Ar}/^{39}\text{Ar}$ dating allows us to resolve the admixture of phenocryst-hosted inherited ^{40}Ar in the
482 final temperature steps of the incremental step heating experiments. More than half of our $^{40}\text{Ar}/^{39}\text{Ar}$ ages derived for this study
483 are based on this method. All incremental step heating experiments are reproducible, except for the sample G15M0017 which
484 gave the oldest age. The total fusion experiments of this study gave at least five times smaller analytical uncertainty (1SE on
485 average ≤ 0.01 Ma) than the previous studies using conventional K-Ar (Angelier et al., 1977; Fytikas et al., 1976, 1986; Matsuda
486 et al., 1999) and SHRIMP U/Pb zircon methods (Stewart and McPhie, 2006). Fission track dating on obsidians of the Milos
487 VF produced two ages (Bigazzi and Radi, 1981; Arias et al., 2006) which seems to overlap with the K-Ar and $^{40}\text{Ar}/^{39}\text{Ar}$ ages,
488 but with larger uncertainty. U/Pb zircon ages could indicate the timing of zircon formation at high temperature (>1000 °C) in
489 magma chambers significantly prior to volcanic eruption (e.g. Flowers et al., 2005). On the other hand, the lower closure
490 temperature of K-rich minerals (<700 °C) makes the K-Ar and $^{40}\text{Ar}/^{39}\text{Ar}$ ages better suited to determine the timing of extrusion
491 of volcanic products (e.g. Grove and Harrison, 1996; Cassata and Renne, 2013).

492 The MSWD value, as a measure of the scatter of the individual step ages, is based on the error enveloping around the data
493 point. The decrease in error will automatically cause an increase in MSWD (e.g. York, 1968; Wendt and Carl, 1991). The
494 MSWD values reported in this study are relatively high. In part this is caused by the fact that modern multi-collector mass
495 spectrometers used for $^{40}\text{Ar}/^{39}\text{Ar}$ dating can measure the isotope ratios very precisely, which in turn would increase the MSWD.
496 It will be more valuable and challenging to find a plateau or isochron age which meets the MSWD criteria (<2.5) by modern
497 multi-collector $^{40}\text{Ar}/^{39}\text{Ar}$ dating than by K-Ar or $^{40}\text{Ar}/^{39}\text{Ar}$ dating using a single detector instrument (e.g. Mark et al., 2009).
498 Potential drawbacks of the $^{40}\text{Ar}/^{39}\text{Ar}$ method are its dependence on neutron irradiation causing the production of interfering
499 argon isotopes that need to be corrected for. The uncertainty in the ages of standards that are required to quantify the neutron
500 flux also needs to be incorporated in the final ages as are uncertainties related to decay constants (supplementary material II).
501 Finally, recoil can occur during irradiation. Minerals such as biotite can be prone to recoil, yielding slightly older ages (e.g.
502 Hora et al., 2010).

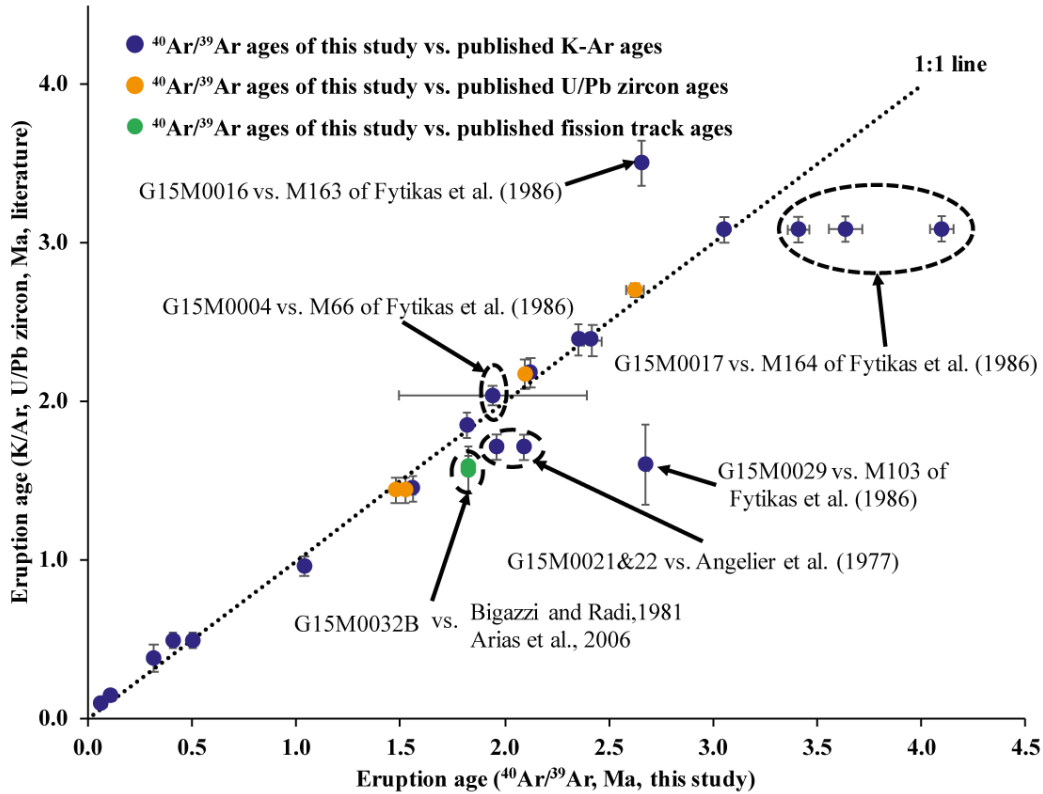
503 Figure 12 compares previous published K-Ar, U/Pb zircon and fission track ages from the same volcanic units with the new
504 $^{40}\text{Ar}/^{39}\text{Ar}$ data of this study. In general, there is a good agreement, however, six ages out of twenty-three differ significantly
505 from previous studies and will be discussed below.

506 The obsidian fission track ages (Bigazzi and Radi, 1981; Arias et al., 2006) for the Dhemenehaki volcano are 0.25 My younger
507 than the K-Ar ages (1.84 Ma, Angelier et al., 1977) and the $^{40}\text{Ar}/^{39}\text{Ar}$ age of this study (1.825 Ma, G15M0032B). The good
508 agreement between the K-Ar and $^{40}\text{Ar}/^{39}\text{Ar}$ ages suggests that the fission track ages record another, lower temperature event,
509 than the K-Ar and $^{40}\text{Ar}/^{39}\text{Ar}$ ages. In addition, the larger uncertainty of fission track ages (>0.05 Ma) also overlaps with the
510 $^{40}\text{Ar}/^{39}\text{Ar}$ age at 2-sigma. We assume that the $^{40}\text{Ar}/^{39}\text{Ar}$ age is the correct extrusion age for the obsidian of the Dhemenehaki
511 volcano.

512 Angelier et al. (1977) reported one dacite sample in the northwest of Milos with an age of 1.71 Ma (Angelier_3, location 3 on
513 Figure 3 of Angelier et al., 1977). Argon loss could result in these ages (Angelier_3-5 in Figure 12) being younger than our
514 $^{40}\text{Ar}/^{39}\text{Ar}$ groundmass ages of 1.97 ± 0.01 Ma (dacite sample G15M0021 and -22).

515 The amphibole of sample G15M0004 of the Adamas dacitic lava dome, located ~ 1 km north of rhyolitic Bombarda volcano,
516 gave an inverse isochron age of $1.95 \text{ Ma} \pm 0.45 \text{ Ma}$. This age overlaps with the K-Ar age for the Adamas lava dome of $2.03 \pm$
517 0.06 Ma (dacite M 66) of Fytikas et al. (1986). The large analytical uncertainty of our sample G15M0004 is caused by a

518 combination of low $^{40}\text{Ar}^*$ yields and clustering of data points that define the inverse isochron showing excess argon was
 519 identified by the $^{40}\text{Ar}/^{39}\text{Ar}$ method ($^{40}\text{Ar}/^{36}\text{Ar}$ 319.51 ± 14.70), whereas the presence of excess argon cannot be tested by the
 520 K-Ar technique, implying that the Fytikas et al. (1986) might be slightly old.



521
 522 **Figure 12.** The $^{40}\text{Ar}/^{39}\text{Ar}$ ages of this study (x-axis) compared to the K/Ar ages (Angelier et al., 1977; Fytikas et al., 1986), U/Pb
 523 zircon ages (Stewart and McPhie, 2006) and fission track ages (Bigazzi and Radi, 1981; Arias et al., 2006) (y-axis) for the same
 524 volcanic units. Ages which deviate from the 1:1 correlation line are discussed in section 4.1.

525 The Korakia andesite has an age of 1.59 ± 0.25 Ma (M 103, Fytikas et al., 1986) and was deposited in a submarine-subaerial
 526 environment on top of the Sarakiniko Formation that was dated based on paleomagnetic polarity in combination with a K-Ar
 527 age (1.80-1.85 Ma, Stewart and McPhie, 2003 and reference therein). The much older $^{40}\text{Ar}/^{39}\text{Ar}$ groundmass age (2.68 ± 0.01
 528 Ma) of Korakia andesite sample G15M0029 is unreliable and it could indicate the emplacement age of the Kalogeros
 529 cryptodome (2.70 ± 0.04 Ma, Stewart and McPhie, 2006) or represents a geological meaningless age with only 23-27% of the
 530 total ^{39}Ar released in the “plateau”. In this case, the K-Ar age of 1.59 ± 0.25 Ma is considered as the likely eruption age for the
 531 Korakia andesite although its argon loss or excess Ar component is unknown.

532 We obtained $^{40}\text{Ar}/^{39}\text{Ar}$ ages of 3.41-4.10 Ma and 3.06 ± 0.02 Ma, respectively, from the groundmasses of dacite samples
 533 G15M0017 and G15M0015 in the southwest of Milos (Figure 2 and 13B). Both of these samples are derived from the coherent
 534 dacite facies of the rhyolitic Profitis Illias volcano based on the Figure 11 of Stewart and McPhie (2006). Sample G15M0015
 535 yielded much higher radiogenic ^{40}Ar (41.77%) than that of sample G15M0017 (<10% of $^{40}\text{Ar}^*$), and the rhyolite sample M
 536 164 from Fytikas et al. (1986) (23.5% of $^{40}\text{Ar}^*$) gave an estimate the eruptive age of 3.08 ± 0.08 Ma to the Profitis Illias
 537 volcano which is much younger than that given by our sample G15M0017 (Figure 12). Therefore, we consider our $^{40}\text{Ar}/^{39}\text{Ar}$
 538 ages of 3.06 ± 0.02 Ma as the best estimate of the emplacement age of the coherent dacite facies of Profitis Illias volcano.

539 A basaltic andesite dyke near Kleftiko on the south-western coast of Milos has a K-Ar age of 3.50 ± 0.14 Ma which only gave
 540 13.9% of $^{40}\text{Ar}^*$ (Fytikas et al. 1986). This age is significantly older than the eruptive ages of Profitis Illias volcano which the
 541 dyke intruded (Stewart, 2003). Although containing relatively low $^{40}\text{Ar}^*$ (16.87%), our $^{40}\text{Ar}/^{39}\text{Ar}$ age of 2.66 ± 0.01 Ma with
 542 67.27% of $^{40}\text{Ar}^*$ from the groundmass of basaltic andesitic sample G15M0016 of the dyke near Kleftiko is probably an accurate
 543 intrusion age.

544 4.2 The published ages of other volcanic units

545 Unfortunately, we were not able to date all key volcanic units of the Milos VF. This was due to three reasons: (1) we did not
546 collect samples from all units; (2) some of the collected samples were not fresh enough after inspection of thin sections; and
547 (3) some of the $^{40}\text{Ar}/^{39}\text{Ar}$ data indicate that the K-Ar decay system was disturbed. Therefore, we include published age
548 information to establish a complete high-resolution geochronology for the Milos VF.

549 The published volcanic units that we include are the Profitis Illias volcano (3.08 ± 0.08 Ma with 23.5 (%), Fytikas et al., 1986),
550 the Mavro Vouni lava dome (2.50 ± 0.09 Ma with 55.2 $^{40}\text{Ar}^*$ (%), Anglier et al., 1977) in the south-western part of Milos, the
551 Bombarda volcano (1.71 ± 0.05 Ma with 24.3 $^{40}\text{Ar}^*$ (%), Fytikas et al., 1986), the Plakes volcano (0.97 ± 0.06 Ma with 10.2
552 $^{40}\text{Ar}^*$ (%), Fytikas et al., 1986, and 0.8-1.2 Ma with 5.4-11.9 $^{40}\text{Ar}^*$ (%) Matsuda et al. 1999). Scoria deposits that Stewart and
553 McPhie (2006) attributed to an andesitic scoria cone between Milos and Kimolos were produced in submarine, and maybe
554 occasionally above sea level. No age data for this deposit has been published so far. However, the stratigraphic position of this
555 scoria deposit is between MIL 365 (2.66 Ma, Stewart and McPhie, 2006) and M103 (1.59 Ma, Fytikas et al., 1986), which is
556 shown in Figure 10 of Stewart and McPhie (2006). Therefore, this scoria cone was likely active in the north-eastern part of the
557 Milos VF between 2.6 and 1.6 Ma.

558 Fytikas et al. (1986) also analysed a pumice coming from the Sarakiniko deposits east of Adamas (1.85 ± 0.10 Ma with 13.6
559 $^{40}\text{Ar}^*$ (%), Fytikas et al., 1986) (Fig. 2). This unit is reworked pyroclastic sediment of the Adamas lava dome (Rinaldi and
560 Venuti, 2003). Therefore, the K-Ar age from the Sarakiniko unit is not considered as an eruption age in this study. We did not
561 sample the neighbouring islands of the Milos VF and also did not attempt to date the products of the recent phase of phreatic
562 activity from which Traineau and Dalabakis (1989) obtained ^{14}C ages of 200 BC and 200 AD.

563 4.3 Implications for the stratigraphy of the Milos VF

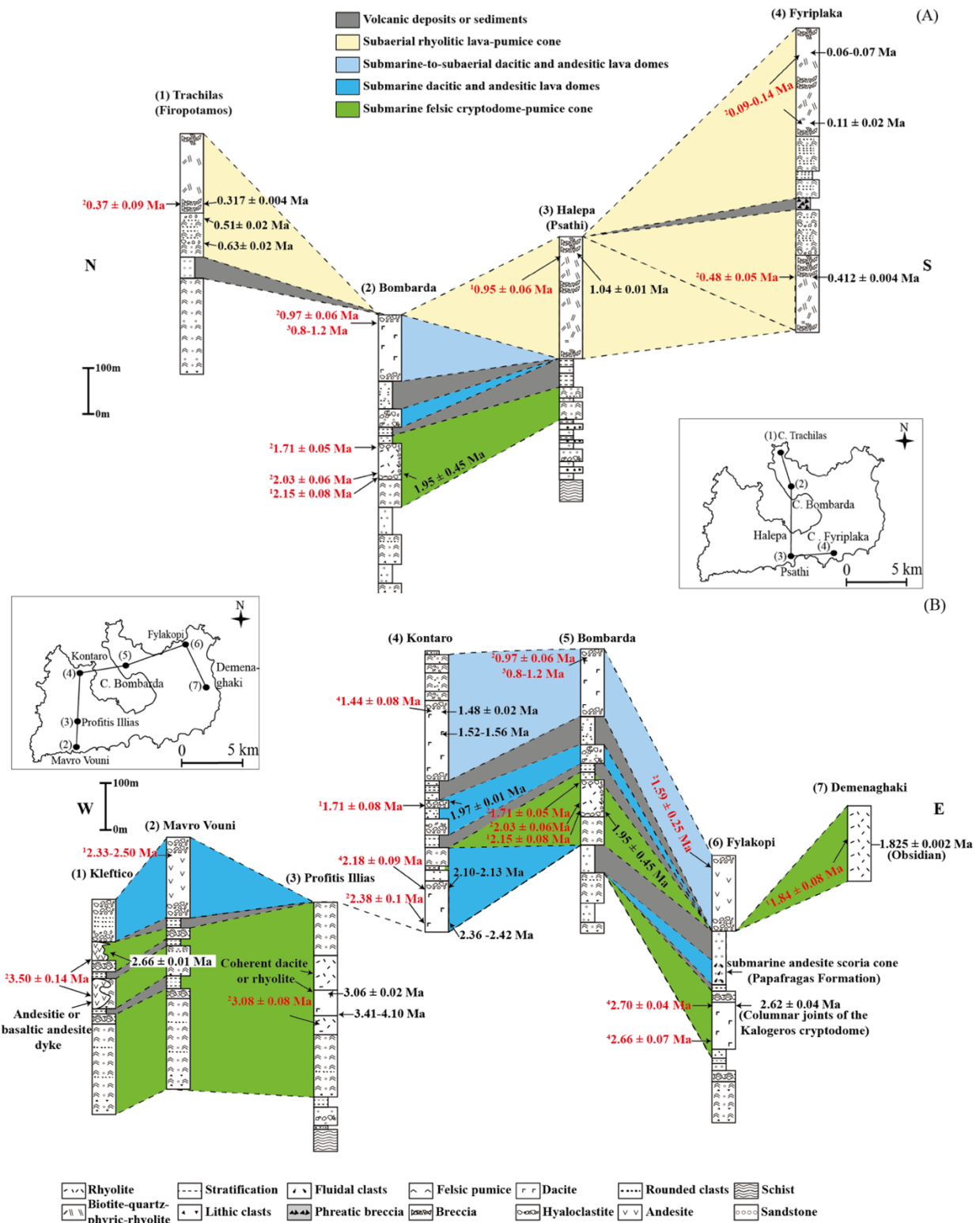
564 4.3.1. Start of volcanism in the Milos VF

565 Figures 13 and 14 summarize our new $^{40}\text{Ar}/^{39}\text{Ar}$ ages in combination with previously published stratigraphic, biostratigraphic,
566 fission track, ^{14}C , K-Ar and U-Pb age data. We did not consider the Matsuda et al. (1999) data as the fission-track ages seem
567 to be offset to other dating techniques ages obtained from the same deposits (see section 4.1 above). The exact start of
568 volcanism in the Milos VF is still unclear since these older deposits are strongly hydrothermally altered. Van Hinsbergen et al.
569 (2004) reported five ash layers in the Pliocene sedimentary rocks of southern Milos, ranging between 4.5-3.7 Ma in age, based
570 on biostratigraphy, magnetostratigraphy and astronomical dating. In a slightly wider circle around Milos island, the $6.943 \pm$
571 0.005 Ma a1-tephra event recorded in several locations on nearby Crete (Rivera et al., 2011) shows that explosive volcanism
572 along the Aegean arc, possibly on Milos, already occurred during the Messinian. These ash beds cannot be traced to currently
573 exposed centres in the Milos VF and could conceivably be related to volcanic centres further north (Antiparos and Patmos),
574 which were active during this time interval (Vougioukalakis et al., 2019).

575 Biostratigraphy shows that the youngest layer with dateable fossils (bio-event, the last common occurrence of *Sphenolithus*
576 spp., Van Hinsbergen et al., 2004) in the Neogene sedimentary rocks is 3.61 Ma old (GTS2020, Raffi et al., 2020). The
577 diatomite Unit II from Calvo et al. (2012) on top of the oldest volcanoclastic deposit from the north-eastern coast of Milos is
578 constrained within 2.83-3.19 Ma. These data suggest that the oldest products must be older than 2.83 Ma and younger than
579 3.61 Ma. Our oldest $^{40}\text{Ar}/^{39}\text{Ar}$ ages of this study displayed a wide range of 3.41-4.10 Ma that is probably not correct due to
580 alteration of the samples. Alteration might induce Ar loss and that would imply that the age is even older than 3.4-4.1 Ma. The
581 age of 3.50 ± 0.14 Ma given by Fytikas et al. (1986) for an andesitic pillow lava or dyke has been discussed above and probably
582 belongs to a series of basaltic andesite intrusions in the younger dacitic-rhyolitic deposits of Profitis Illias (~ 3.08 Ma, Fytikas
583 et al., 1986), and therefore the 3.5 Ma age is probably not correct (e.g. Stewart, 2003). Fytikas et al. (1986) measured one
584 sample from Kimolos (Figure 2 and 3) with an age of 3.34 Ma. Furthermore, Ferrara et al. (1980) reported an age of 3.15 Ma

585 for a lithic clast derived from the Petalia intrusion in the Kastro volcanoclastics of Polyegos. If we assume that this reported
 586 age is a cooling age, volcanism in the Milos VF must have started before 3.15 Ma. Although age constraints for the start of
 587 volcanism on Milos both from the Neogene sedimentary rocks and the dated volcanic samples are poor, the evidence at this
 588 stage would suggest that volcanism in the Milos VF started ~3.3 Ma ago.

589



590

591 **Figure 13.** Nine selected stratigraphic columns covering the (A) young (<1.4 Ma) and (B) old (>1.4 Ma) volcanic deposits of Milos
 592 modified after Stewart and McPhie (2006), except for (7) Demenaghaki. Age data in black are from this study and in red are from:
 593 1=Angelier et al. (1977), 2=Fytikas et al. (1976, 1986), 3=Matsuda et al. (1999), 4=Stewart and McPhie (2006).

594

595 **4.3.2. Periods with different volumetric output**

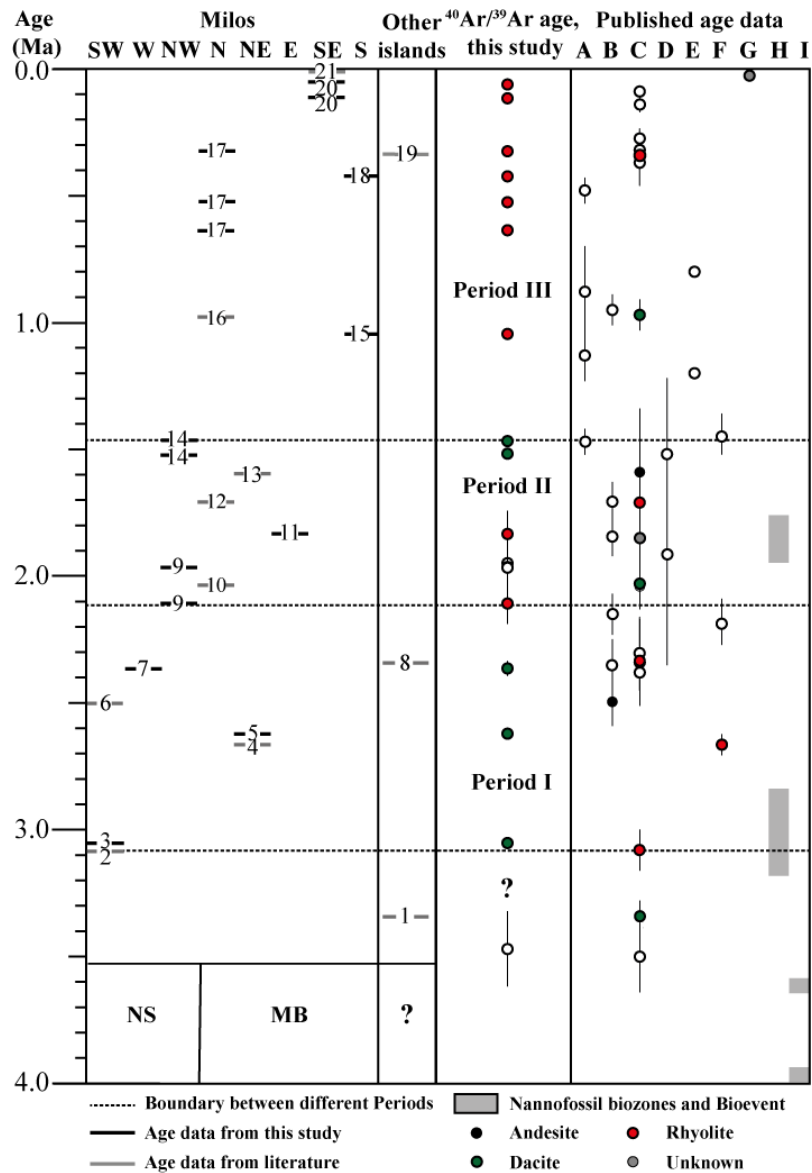
596 The volume estimates of the Milos VF are hampered by limited exposure of several volcanic units and unknown age
 597 relationships. Therefore, not all units can be attributed to a certain volcano. Furthermore, we also do not know how much the
 598 volcanic products were lost through transport by air, sea currents and erosion. Therefore, the discussion here only provides a
 599 first order estimate of the onshore extruded magma volume. Taken into account all these limitations, our age data and the
 600 volume estimates by Stewart and McPhie (2006) indicate at least three periods of different long-term volumetric volcanic
 601 output rates (Q_e) from ~3.3 to 0.0 Ma. We define a “Period” as a time interval where the Q_e is significantly different from the
 602 average output rate (Q_e average = $1.0 \times 10^{-5} \text{ km}^3 \cdot \text{yr}^{-1}$) of the Milos VF over the last 3.3 Ma. Figure 11 shows that the Q_e can be
 603 subdivided into two slow-growth periods (I and III) and one period (II) during which the Q_e was significantly larger.
 604 The lower boundary of Period I is based on our estimate of the oldest volcanic units of Milos at ~3.3 Ma. These oldest units
 605 were deposited in the southwest of Milos between ~3.3 and 3.08 Ma and include the BPS of Fytikas et al. (1986) and the felsic
 606 pumice cone/crypto dome facies of Stewart and McPhie (2006). These deposits have a minimum thickness of 120 m. The
 607 estimates of the DRE volume and Q_e of these earliest volcanic deposits are hampered by the lack of precise age information,
 608 the high degree of alteration and structural complexities. Therefore, we only calculated the Q_e of Period I from 3.08 Ma for
 609 which the eruption products are mainly dacitic-rhyolitic in composition (Table 5, Fig 11), and the first products that can be
 610 reliably dated are cryptodomes (3.06 Ma, sample G15M0015) and dykes (2.66 Ma, sample G15M0016) into the BPS of Fytikas
 611 et al. (1986) or the units of Profitis Illias volcano of Stewart and McPhie (2006, 3.08 Ma) in the southwest of Milos. These
 612 cryptodomes and dykes were followed by the formation of the submarine Fylakopi pumice cone volcano at 2.66 Ma (Stewart
 613 and McPhie, 2006) and Kalogeros cryptodome at 2.62 Ma (sample G15M0006) in the north-eastern part of Milos. These two
 614 pumice cone volcanoes contributed 3-11 km^3 DRE in volume to the Milos VF. The last two volcanic activities of Period I
 615 occurred in the southwest (Mavro Vauni, 2.50 Ma, Angelier et al., 1977) and west of Milos (Mavros Kavos, 2.36 Ma, this
 616 study), respectively, which produced two high-aspect-ratio andesitic-dacitic lava domes with a total volume of 1-3 km^3 DRE
 617 (Stewart and McPhie, 2006). During the submarine Period I, which lasted ~ 1.2 Ma, the estimated Q_e is $0.9 \pm 0.5 \times 10^{-5} \text{ km}^3 \cdot \text{yr}^{-1}$.
 618 ¹.

Table 5. Summary of the eruption ages of the Milos volcanic field

No.	Name of volcanic centre	Age (Ma)	Reference
1	Kimlos volcano	3.34	Fytikas et al., 1986
2	Profitis Illias crypto/pumice cone	3.08	Fytikas et al., 1986
3	coherent dacite of Profitis Illias volcano	3.06	This study
4	Filakopi volcano	2.66	Stewart and McPhie, 2006
5	Kalegeros cryptodome	2.62	This study
6	Mavro Vouni lava dome	2.5	Angelier et al., 1977
7	Mavros Kavos lava dome	2.42-2.36	This study
8	Polyegos lava dome	2.34	Fytikas et al., 1986
9	Triades lava dome	2.13-2.10 and 1.97	This study
10	Adamas lava dome	2.03	Fytikas et al., 1986
11	Dhemeneghaki volcano	1.83	This study
12	Bombardo volcano	1.71	Fytikas et al., 1986
13	Korakia dome	1.59	Fytikas et al., 1986
14	Komntaro dome	1.52-1.48	This study
15	Halepa lava dome	1.04	This study
16	Plakes lava dome	0.97	Fytikas et al., 1986
17	Trachilias complex	0.63, 0.51 and 0.317	This study
18	Kalamos lava dome	0.41	This study
19	Antimilos domes	0.32	Fytikas et al., 1986
20	Fyriplaka complex	0.11 and 0.07-0.06	This study
21	Phreatic activity	200 AD-200 BC	Trainau and Dalabakis, 1989

619
 620 The change from Period I to II is based on the sharp increase in Q_e at 2.13 Ma (Fig. 11). During this period the Q_e ($3.0 \pm$
 621 $1.7 \times 10^{-5} \text{ km}^3 \cdot \text{yr}^{-1}$) increased by a factor of ~3 compared to Period I and III. Period II began with the submarine extrusions of
 622 the dacitic-rhyolitic Triades lava dome in the north-west and dacitic Adamas lava dome in the north-east of Milos and was

623 followed by the rhyolitic Dhemenehaki pumice cone/cryptodome and the Bombardo volcano in the north-east of Milos. For
624 the Bombarda centre a large age range is reported in the literature (1.71-2.15 Ma, Fig. 13B). We did not successfully date
625 samples from the Bombarda centre, but Rinaldi and Campos Venuti (2003) reported that an age of 1.71 Ma is the best
626 approximation based on other stratigraphic information. For the Dhemenehaki centre, we obtained a $^{40}\text{Ar}/^{39}\text{Ar}$ age of 1.825
627 ± 0.002 Ma from obsidian. The Triades, Adamas, Dhemenehaki and Bombarda centres all developed in submarine settings,
628 as the intercalated sediments from the northern coast of Milos show (Calvo et al., 2012; Fig. 14). The last two volcanic
629 expressions in Period II consist of two submarine-to-subaerial lava dome extrusions, Kantaro (1.59 Ma, Fytikas et al., 1987)
630 and Korakia (1.48 Ma, this study) in the north-west and north-east of Milos, respectively. The products of these two centres
631 are andesitic-dacitic in composition. All volcanic centres of Period II produced 8-30 km³ DRE in volume for the Milos VF.
632 Period III began with a time interval of 0.4 Ma with no eruptions and has a very low Q_e of $0.25 \pm 0.05 \times 10^{-5}$ km³·yr⁻¹. The
633 boundary between Period II and III can be placed at the last eruption of Period II, at the start of the first eruption in the low
634 output interval, or halfway in between. The difference between those options is not significant, given the large uncertainties
635 of the volume estimates (Fig. 12), and therefore we have decided to start Period III directly after the last eruption of the high
636 Q_e of Period II. The composition of nearly all Period III volcanic products is rhyolitic, an exception is the dacitic Plakes lava
637 dome (Fig. 12). The Plakes lava dome is probably the last volcano erupting at ~ 0.97 Ma (Fytikas et al., 1987) in a submarine
638 environment in the north of Milos, whereas the other lava dome in Period III, Halepa, produced rhyolitic lavas in a subaerial
639 setting in the south (Stewart and McPhie, 2006). The Halepa and Plakes domes contributed 1-3 km³ DRE in volume to the
640 Milos VF and were followed by a 0.3 Ma interval with no or limited volcanic eruptions. Two subaerial pumice cone volcanoes
641 with biotite bearing rhyolites were constructed during the last 0.6 Ma, the Trachilias and Fyriplaka complexes. The Trachilias
642 complex was active for approximately 300 kyr (0.63-0.32 Ma) in the northern part of Milos. The evolution of this complex
643 began with phreatic eruptions which became less explosive over time (Fytikas et al., 1986). During the last eruption ($0.317 \pm$
644 0.004 Ma) of the Trachilias complex rhyolitic pumices filled up the crater area and did breach the northern tuff cone walls. The
645 Trachilias complex only added a small volume (1-2 km³ DRE) to the Milos VF. The Kalamos lava dome was also extruded in
646 the south of Milos (Fig. 2) contemporaneously with the Trachilias complex.
647 The youngest volcanic activity of Milos (0.11 Ma-present) is characterized by subaerial eruptions of biotite phyric rhyolite
648 from the Fyriplaka complex in the south of Milos, and was studied in detail by Campos Venuti and Rossi (1996). This complex
649 is constructed on a paleosol that developed in a phreatic deposit ("Green Lahar", Fytikas et al., 1986) or lies directly on the
650 metamorphic basement. Campos Venuti and Rossi (1996) indicated that the stratigraphic order is: Fyriplaka and Gheraki tuff
651 rings, Fyriplaka lava flow, tuff cone of Tsigrado-Provatas. The total estimated volume of volcanic material is 0.18 km³ DRE.
652 The boundary between the Fyriplaka and Tsigrado tuff cones is characterized by a marked erosive unconformity. The
653 composition of these young volcanic products is very constant (Fig. 10-11), as noted by Fytikas et al. (1986) and Campos
654 Venuti and Rossi (1996). The products from Fyriplaka and Tsigrado cones are covered by a paleosol rich in archaeological
655 remains and a phreatic deposit consisting largely of greenschist metamorphic fragments. According to Campos Venuti and
656 Rossi (1996), the Fyriplaka cone was quickly built by phreatic and phreatomagmatic eruptions, as there are no paleosols
657 observed between the different units. However, our data do suggest a large range in ages between 0.11 and 0.06 Ma. Fytikas
658 et al. (1986) also reported a range between 0.14 and 0.09 Ma. These ages are inconsistent with the "Green Lahar" age of 27
659 kyrs (Principe et al., 2002), suggesting that the "Green Lahar" deposit consists of many different phreatic eruption layers that
660 were formed during a time interval of more than 0.4 Ma, as the Kalamos lava is underlain by a green phreatic eruption breccia
661 (Campos Venuti and Rossi 1996). We, therefore, conclude that phreatic eruptions occurred for more than 400 kyr,
662 predominantly in the eastern part of Milos until historical times (200 BC – 200 AD, Traineau and Dalabakis, 1989).



663
664
665
666
667
668
669
670
671
672
673
674
675

Figure 14. Diagram presenting three periods of different long-term volumetric volcanic output rate on Milos volcanic field based on the new $^{40}\text{Ar}/^{39}\text{Ar}$ data of this study and published data. The location of the different volcanoes is given in Fig 2 and indicated in the left panel (from left to right: SW, W, NW, N, NE, E, SE and S of Milos). The right panel corresponds to published age data: [A]=Fytikas et al., 1976, [B]=Angelier et al., 1977, [C]=Fytikas et al., 1986, [D]= Bigazzi & Radi, 1981, [E]=Matsuda, 1999, [F]=Stewart and McPhie (2006), [G]= Trainau and Dalabakis, 1989, and Biostratigraphic data of the Neogene sediments (NG) is from [H]=Calvo et al. (2012) and [I]=Van Hinsbergen et al. (2004) calibrated to Raffi et al. (2020) (LCO of *Sphenolithus* spp. and FO of *D. tamalis*). The number in the left panel represents the volcanic centres of Milos (see details in Table 5). The start of volcanism (3.08-3.61 Ma) on Milos and the basement of the other Islands (Antimilos, Kimolos and Polyegos) are not well constrained and indicated with question marks (see text for discussion). The simplified basement cross-section (NS: Neogene sedimentary rock; MB: Metamorphic basement) under Milos volcanic units is based on Fytikas et al. (1989). We used the filled symbols as the best estimate for the eruption ages at the different volcanic centres, and the open symbols are not used as the best estimate due to their relatively large uncertainties.

676

4.3.3 Temporal evolution of the magma flux and composition

677
678
679
680
681
682
683

Figure 11 shows temporal major-element variations during the evolution of the Milos VF. The volcanic units of Period III are dominantly rhyolitic in composition, whereas during Period I and II the compositions of volcanic units range between basaltic-andesite to rhyolite. However, the $\text{K}_2\text{O}/\text{SiO}_2$ ratio is constant (0.05 ± 0.02) over the 3.3 Ma evolution of the Milos VF, with one exception, sample G15M0021 collected near Cape Vani which is altered by hydrothermal processes (e.g. Alfieris et al. 2013). Period I and III contain large explosive pumice cone volcanoes, whereas Period II is dominated by effusive dome extrusions. The difference in volcanic structures is not observed in the SiO_2 content and the $\text{K}_2\text{O}/\text{SiO}_2$ ratio of the volcanic products.

684 It is noteworthy that the value of the Q_e ($0.2-4.7 \times 10^{-5} \text{ km}^3 \cdot \text{yr}^{-1}$) for the Milos VF is at least 2-3 orders lower than the average
685 for rhyolitic systems ($4.0 \times 10^{-3} \text{ km}^3 \cdot \text{yr}^{-1}$) and the mean for continental arcs ($\sim 70 \times 10^{-3} \text{ km}^3 \cdot \text{yr}^{-1}$) (White et al., 2006). Milos
686 overlaps with the lowest Q_e values of the study of White et al. (2006). No data are available for the ratio between intruded
687 magma in the crust below Milos and extruded volcanic units (I:E). White et al. (2006) argued that a ratio of 5:1 (I:E) is probably
688 a realistic estimate for most volcanic centres and that this ratio can be higher in volcanic centres constructed on continental
689 crust. A magma supply rate from the mantle beneath the Milos VF could be estimated in the order of $0.1-3.3 \times 10^{-4} \text{ km}^3 \cdot \text{yr}^{-1}$.
690 Druitt et al. (2019) reported a long-term average magma supply rate of approximately $1 \times 10^{-3} \text{ km}^3 \cdot \text{yr}^{-1}$ beneath the Kameni
691 islands of Santorini, which is comparable to that of the Milos. Besides the case of Santorini VF, no other information on the
692 long-term average magma supply rate of other volcanic centres of the SAVA is available to our knowledge.
693 Milos is approximately 15 km long (W-E), a magma production rate of approximately $0.7-22 \text{ km}^3 \cdot \text{km}^{-1} \cdot \text{Ma}^{-1}$ can be estimated
694 over the last ~ 3.34 Ma. Although this magma production rate per km arc length is the onshore estimate for the Milos VF, it is
695 still significantly lower than for oceanic arcs: $157-220 \text{ km}^3 \cdot \text{Ma}^{-1} \cdot \text{km}^{-1}$ (Jicha and Jagoutz, 2015). For continental arcs, the long-
696 term magma production rate is more difficult to establish because magmatism is cyclic, and short periods (5-20 Ma) of intense
697 magmatism (“flare ups”) with $85 \text{ km}^3 \cdot \text{km}^{-1} \cdot \text{Ma}^{-1}$ being alternated with periods of 25-50 Ma of low magma production rate of
698 $20 \text{ km}^3 \cdot \text{km}^{-1} \cdot \text{Ma}^{-1}$ (e.g. Jicha and Jagoutz, 2015). The periods of low magma production overlap with the magma production
699 rates beneath the Milos VF over the past ~ 3.34 Ma.

700 5 Conclusions

701 This study reports twenty-one new $^{40}\text{Ar}/^{39}\text{Ar}$ ages and major element data for 10 volcanic units of the Milos Volcanic Field.
702 In combination with previously published age data, geochemistry and facies analysis the following points can be made.

- 703 (1) The exact age of the start of volcanism in the Milos VF is still unclear due to the high degree of alteration of the oldest
704 deposits. The best estimate based on our new $^{40}\text{Ar}/^{39}\text{Ar}$ ages, published K-Ar data and nannofossil biozones is between
705 3.5 and 3.15 Ma.
- 706 (2) Based on the long-term volumetric volcanic output rate, the volcanic history of the Milos VF can be divided into two
707 slow growth periods, Period I ($\sim 3.3-2.13$ Ma) and III (1.48 Ma-present), and one relatively fast growth period, Period
708 II (2.13-1.48 Ma).
- 709 (3) Period I and II are characterised by andesitic to rhyolitic lavas and pyroclastic units, whereas those of Period III are
710 dominantly rhyolitic. The $\text{K}_2\text{O}/\text{SiO}_2$ ratio is constant over the 3.3 Ma history of the Milos VF.
- 711 (4) The long-term volumetric volcanic output rate of Milos is $0.2-4.7 \times 10^{-5} \text{ km}^3 \cdot \text{yr}^{-1}$, two-three orders of magnitude lower
712 than the average for rhyolitic systems and continental arcs.

713 Acknowledgement

714 We would like to thank Roel van Elsas for the assistance with rock crushing and mineral separation. Kiki Dings helped with
715 the XRF bead preparation and measurements. Lara Borst and Onno Postma assisted with the $^{40}\text{Ar}/^{39}\text{Ar}$ dating. We acknowledge
716 the Greek Institute of Geology and Mineral Exploration (IGME) for permission to conduct fieldwork on Milos. Xiaolong Zhou
717 would like to acknowledge a grant no. 201506400055 from the China Scholarship Council (CSC). The $^{40}\text{Ar}/^{39}\text{Ar}$ facility of the
718 VU is covered by NWO grant 834.09.004. This research benefitted from funding from the European Research Council under
719 the European Union's Seventh Framework Programme (FP7/2007-2013)/ERC grant agreement n° 319209. A previous version
720 of this manuscript greatly benefitted from a very detailed and constructive review by Dr. J. McPhie. A second review by Dr J.
721 McPhie, Dr. J-F. Wotzlaw and Dr. Peter Abbott helped to clarify the interpretation of the geochronology of Milos. We thank
722 Drs. J. Nadden, J. Miles and S Tapster for pointing out mistakes in our figures.

- 724 Alfieris, D., Voudouris, P. and Spry, P. G.: Shallow submarine epithermal Pb-Zn-Cu-Au-Ag-Te mineralization on western
725 Milos Island, Aegean Volcanic Arc, Greece: Mineralogical, geological and geochemical constraints, *Ore Geol. Rev.*, 53,
726 159–180, doi:10.1016/j.oregeorev.2013.01.007, 2013.
- 727 Angelier, J., Cantagrel, J.-M. and Vilminot, J.-C.: Neotectonique cassante et volcanisme plio-quadernaire dans l'arc egeen
728 interne; l'île de Milos (Grece), *Bull. la Société Géologique Fr.*, 7(1), 119–124, 1977.
- 729 Arias, A., Oddone, M., Bigazzi, G., Di Muro, A., Principe, C. and Norelli, P.: New data for the characterization of Milos
730 obsidians, *J. Radioanal. Nucl. Chem.*, 268(2), 371–386, doi:10.1007/s10967-006-0183-9, 2006.
- 731 Berger, G. W. and York, D.: Geothermometry from $^{40}\text{Ar}/^{39}\text{Ar}$ dating experiments, *Geochim. Cosmochim. Acta*, 45(6), 795–
732 811, doi:10.1016/0016-7037(81)90109-5, 1981.
- 733 Bigazzi, G. and Radi, G.: Datazione con le tracce di fissione per l'identificazione della provenienza dei manufatti di
734 ossidiana, *Riv. di Sci. Preist.*, 36/1–2, 223–250, 1981.
- 735 Calvo, J. P., Triantaphyllou, M. V., Regueiro, M. and Stamatakis, M. G.: Alternating diatomaceous and volcanoclastic
736 deposits in Milos Island, Greece. A contribution to the upper Pliocene-lower Pleistocene stratigraphy of the Aegean Sea,
737 *Palaeogeogr. Palaeoclimatol. Palaeoecol.*, 321–322, 24–40, doi:10.1016/j.palaeo.2012.01.013, 2012.
- 738 Campos Venuti, M. and Rossi, P. L.: Depositional facies in the Fyriplaka rhyolitic tuff ring, Milos Island (Cyclades, Greece),
739 *Acta Vulcanol.*, 8, 173–192, 1996.
- 740 Cassata, W. S. and Renne, P. R.: Systematic variations of argon diffusion in feldspars and implications for
741 thermochronometry, *Geochim. Cosmochim. Acta*, 112, 251–287, doi:10.1016/j.gca.2013.02.030, 2013.
- 742 Cole, P. D., Calder, E. S., Sparks, R. S. J., Clarke, A. B., Druitt, T. H., Young, S. R., Herd, R. A., Harford, C. L. and Norton,
743 G. E.: Deposits from dome-collapse and fountain-collapse pyroclastic flows at Soufrière Hills Volcano, Montserrat, *Geol.*
744 *Soc. London, Mem.*, 21(1), 231–262, 2002.
- 745 Crosweller, H. S., Arora, B., Brown, S. K., Cottrell, E., Deligne, N. I., Guerrero, N. O., Hobbs, L., Kiyosugi, K., Loughlin,
746 S. C. and Lowndes, J.: Global database on large magnitude explosive volcanic eruptions (LaMEVE), *J. Appl. Volcanol.*,
747 1(1), 4, 2012.
- 748 Druitt, T. H., Edwards, L., Mellors, R. M., Pyle, D. M., Sparks, R. S. J., Lanphere, M., Davies, M. and Barreirio, B.:
749 Santorini Volcano, *Geol. Soc. Mem.*, 19 [online] Available from: <http://pubs.er.usgs.gov/publication/70094778>, 1999.
- 750 Druitt, T. H., Pyle, D. M. and Mather, T. A.: Santorini Volcano and its Plumbing System, *Elements*, 15(3), 177–184,
751 doi:10.2138/gselements.15.3.177, 2019.
- 752 Duermeijer, C. E., Nyst, M., Meijer, P. T., Langereis, C. G. and Spakman, W.: Neogene evolution of the Aegean arc:
753 Paleomagnetic and geodetic evidence for a rapid and young rotation phase, *Earth Planet. Sci. Lett.*, 176(3–4), 509–525,
754 doi:10.1016/S0012-821X(00)00023-6, 2000.
- 755 Ferrara, G., Fytikas, M., Giuliani, O. and Marinelli, G.: Age of the formation of the Aegean active volcanic arc, *Thera*
756 *Aegean world II*, 2, 37–41, 1980.
- 757 Flowers, R. M., Bowring, S. A., Tulloch, A. J. and Klepeis, K. A.: Tempo of burial and exhumation within the deep roots of
758 a magmatic arc, Fiordland, New Zealand, *Geology*, 33(1), 17–20, doi:10.1130/G21010.1, 2005.
- 759 Francalanci, L. and Zellmer, G. F.: Magma Genesis at the South Aegean Volcanic Arc, *Elements*, 15(3), 165–170,
760 doi:10.2138/gselements.15.3.165, 2019.
- 761 Francalanci, L., Vougioukalakis, G. E., Fytikas, M., Beccaluva, L., Bianchini, G. and Wilson, M.: Petrology and
762 volcanology of Kimolos and Polyegos volcanoes within the context of the South Aegean arc, Greece, *Spec. Pap. Soc. Am.*,
763 418, 33, 2007.
- 764 Frey, H. M., Lange, R. A., Hall, C. M. and Delgado-Granados, H.: Magma eruption rates constrained by $^{40}\text{Ar}/^{39}\text{Ar}$
765 chronology and GIS for the Ceboruco-San Pedro volcanic field, western Mexico, *Bull. Geol. Soc. Am.*, 116(3–4), 259–276,

766 doi:10.1130/B25321.1, 2004.

767 Fytikas, M., Giuliani, O., Innocenti, F., Marinelli, G. and Mazzuoli, R.: Geochronological data on recent magmatism of the
768 Aegean Sea, *Tectonophysics*, 31(1–2), T29–T34, doi:10.1016/0040-1951(76)90161-X, 1976.

769 Fytikas, M., 1977. *Geology and Geothermics of Milos Island*. Thesis, Thessaloniki University, 228 pp. (in Greek with
770 English summary).

771 Fytikas, M., Innocenti, F., Kolios, N., Manetti, P., Mazzuoli, R., Poli, G., Rita, F. and Villari, L.: Volcanology and petrology
772 of volcanic products from the island of Milos and neighbouring islets, *J. Volcanol. Geotherm. Res.*, 28(3–4), 297–317,
773 doi:10.1016/0377-0273(86)90028-4, 1986.

774 Fytikas, M.: Updating of the geological and geothermal research on Milos island, *Geothermics*, 18(4), 485–496,
775 doi:10.1016/0375-6505(89)90051-5, 1989.

776 Grasemann, B., Huet, B., Schneider, D. A., Rice, A. H. N., Lemonnier, N. and Tschegg, C.: Miocene postorogenic extension
777 of the Eocene synorogenic imbricated Hellenic subduction channel: New constraints from Milos (Cyclades, Greece), *Bull.*
778 *Geol. Soc. Am.*, 130(1–2), 238–262, doi:10.1130/B31731.1, 2018.

779 Grove, M. and Harrison, T. M.: $^{40}\text{Ar}^*$ diffusion in Fe-rich biotite, *Am. Mineral.*, 81(7–8), 940–951, 1996.

780 Hayes, G. P., Moore, G. L., Portner, D. E., Hearne, M., Flamme, H., Furtney, M. and Smoczyk, G. M.: Slab2, a
781 comprehensive subduction zone geometry model, *Science* (80-), 362(6410), 58–61, doi:10.1126/science.aat4723, 2018.

782 Hildreth, W. and Lanphere, M. A.: Potassium-argon geochronology of a basalt-andesite-dacite arc system: The Mount
783 Adams volcanic field, Cascade Range of southern Washington, *Geol. Soc. Am. Bull.*, 106(11), 1413–1429, 1994.

784 Hildreth, W., Fierstein, J. and Lanphere, M.: Eruptive history and geochronology of the Mount Baker volcanic field,
785 Washington, *Geol. Soc. Am. Bull.*, 115(6), 729–764, 2003a.

786 Hildreth, W., Lanphere, M. A. and Fierstein, J.: Geochronology and eruptive history of the Katmai volcanic cluster, Alaska
787 Peninsula, *Earth Planet. Sci. Lett.*, 214(1–2), 93–114, doi:10.1016/S0012-821X(03)00321-2, 2003b.

788 Van Hinsbergen, D. J. J., Snel, E., Garstman, S. A., Marunțeanu, M., Langereis, C. G., Wortel, M. J. R. and Meulenkamp, J.
789 E.: Vertical motions in the Aegean volcanic arc: Evidence for rapid subsidence preceding volcanic activity on Milos and
790 Aegina, *Mar. Geol.*, 209(1–4), 329–345, doi:10.1016/j.margeo.2004.06.006, 2004.

791 Hora, J. M., Singer, B. S., Jicha, B. R., Beard, B. L., Johnson, C. M., de Silva, S. and Salisbury, M.: Volcanic biotite-
792 sanidine $^{40}\text{Ar}/^{39}\text{Ar}$ age discordances reflect Ar partitioning and pre-eruption closure in biotite, *Geology*, 38(10), 923–926,
793 doi:10.1130/G31064.1, 2010.

794 IJlst, L.: A laboratory overflow-centrifuge for heavy liquid mineral separation, *Am. Mineral.*, 58, 1088–1093, 1973.

795 Jicha, B. R. and Jagoutz, O.: Magma production rates for intraoceanic arcs, *Elements*, 11(2), 105–112,
796 doi:10.2113/gselements.11.2.105, 2015.

797 Kiliass, S. P., Naden, J., Cheliotis, I., Shepherd, T. J., Constandinidou, H., Crossing, J. and Simos, I.: Epithermal gold
798 mineralisation in the active Aegen volcanic arc: The Profitis Ilias deposits, Milos Island, Greece, *Miner. Depos.*, 36(1), 32–
799 44, doi:10.1007/s001260050284, 2001.

800 Koppers, A. A. P.: ArArCALC-software for $^{40}\text{Ar}/^{39}\text{Ar}$ age calculations, *Comput. Geosci.*, 28(5), 605–619,
801 doi:10.1016/S0098-3004(01)00095-4, 2002.

802 Kornprobst, J., Kienast, J.-R. and Vilminot, J.-C.: The high-pressure assemblages at Milos, Greece, *Contrib. to Mineral.*
803 *Petrol.*, 69(1), 49–63, doi:10.1007/bf00375193, 1979.

804 Kuiper, K. F., Deino, A., Hilgen, F. J., Krijgsman, W., Renne, P. R. and Wijbrans, J. R.: Synchronizing Rock Clocks of
805 Earth History, *Science* (80-), 320(5875), 500–504, doi:10.1126/science.1154339, 2008.

806 Lee, J. K. W.: Ar–Ar and K–Ar Dating BT - *Encyclopedia of Scientific Dating Methods*, edited by W. Jack Rink and J. W.
807 Thompson, pp. 58–73, Springer Netherlands, Dordrecht., 2015.

808 Lee, J. Y., Marti, K., Severinghaus, J. P., Kawamura, K., Yoo, H. S., Lee, J. B. and Kim, J. S.: A redetermination of the

809 isotopic abundances of atmospheric Ar, *Geochim. Cosmochim. Acta*, 70(17), 4507–4512, doi:10.1016/j.gca.2006.06.1563,
810 2006.

811 Mark, D. F., Barfod, D., Stuart, F. M. and Imlach, J.: The ARGUS multicollector noble gas mass spectrometer: Performance
812 for $^{40}\text{Ar}/^{39}\text{Ar}$ geochronology, *Geochemistry, Geophys. Geosystems*, 10(10), 1–9, doi:10.1029/2009GC002643, 2009.

813 Matsuda, J., Senoh, K., Maruoka, T., Sato, H. and Mitropoulos, P.: K-Ar ages of the Aegean the volcanic rocks and arc-
814 trench system their implication for the arc-trench system, *Geochem. J.*, 33, 369–377, 1999.

815 McKenzie, D.: Active tectonics of the Alpine—Himalayan belt: the Aegean Sea and surrounding regions, *Geophys. J. Int.*,
816 55(1), 217–254, 1978.

817 Meulenkamp, J. E., Wortel, M. J. R., van Wamel, W. A., Spakman, W. and Hoogerduyn Strating, E.: On the Hellenic
818 subduction zone and the geodynamic evolution of Crete since the late Middle Miocene, *Tectonophysics*, 146(1–4), 203–215,
819 doi:10.1016/0040-1951(88)90091-1, 1988.

820 Min, K., Mundil, R., Renne, P. R. and Ludwig, K. R.: A test for systematic errors in $^{40}\text{Ar}/^{39}\text{Ar}$ geochronology, *Geochim.*
821 *Cosmochim. Acta*, 64(1), 73–98, 2000.

822 Nicholls, I. A.: Santorini volcano, greece - tectonic and petrochemical relationships with volcanics of the Aegean region,
823 *Tectonophysics*, 11(5), 377–385, doi:10.1016/0040-1951(71)90026-6, 1971.

824 Pe-Piper, G. and Piper, D. J. W.: The South Aegean active volcanic arc: relationships between magmatism and tectonics,
825 *Dev. Volcanol.*, 7(C), 113–133, doi:10.1016/S1871-644X(05)80034-8, 2005.

826 Pe-Piper, G. and Piper, D. J. W.: Neogene backarc volcanism of the Aegean: New insights into the relationship between
827 magmatism and tectonics, *Geol. Soc. Am. Spec. Pap.*, 418(02), 17–31, doi:10.1130/2007.2418(02), 2007.

828 Pe-Piper, G. and Piper, D. J. W.: The effect of changing regional tectonics on an arc volcano: Methana, Greece, *J. Volcanol.*
829 *Geotherm. Res.*, 260, 146–163, doi:10.1016/j.jvolgeores.2013.05.011, 2013.

830 Principe C, Arias A, Zoppi U.: Origin, transport and deposition of a debris avalanche de- posit of phreatic origin on Milos
831 Island (Greece). Montagne Pelee 1902-2002, Explosive Vol- canism in Subduction Zones, Martinique 12-16 May,
832 2002. Abstracts p. 71, 2002.

833 Raffi, I., Wade, B. S., Pälke, H., Beu, A. G., Cooper, R., Crundwell, M. P., Krijgsman, W., Moore, T., Raine, I. and
834 Sardella, R.: The Neogene Period, in *Geologic Time Scale 2020*, pp. 1141–1215, Elsevier., 2020.

835 Rinaldi, M. and Venuti, M. C.: The submarine eruption of the Bombarda volcano, Milos Island, Cyclades, Greece, *Bull.*
836 *Volcanol.*, 65(4), 282–293, doi:10.1007/s00445-002-0260-z, 2003.

837 Rivera, T. A., Storey, M., Zeeden, C., Hilgen, F. J. and Kuiper, K.: A refined astronomically calibrated $^{40}\text{Ar}/^{39}\text{Ar}$ age for
838 Fish Canyon sanidine, *Earth Planet. Sci. Lett.*, 311(3–4), 420–426, doi:10.1016/j.epsl.2011.09.017, 2011.

839 Rontogianni, S., Konstantinou, N. S., Melis, C. P. and Evangelidis: Slab stress field in the Hellenic subduction zone as
840 inferred from intermediate-depth earthquakes, *Earth, Planets Sp.*, 63(2), 139–144, doi:10.5047/eps.2010.11.011, 2011.

841 Schaen, A., Jicha, B., Hodges, K., Vermeesch, P., Stelten, M., Mercer, C., Phillips, D., Rivera, T., Jourdan, F., Matchan, E.,
842 Hemming, S., Morgan, L., Kelley, S., Cassata, W., Heizler, M., Vasconcelos, P., Benowitz, J., Koppers, A., Mark, D.,
843 Niespolo, E., Sprain, C., Hames, W., Kuiper, K., Turrin, B., Renne, P., Ross, J., Nomade, S., Guillou, H., Webb, L., Cohen,
844 B., Calvert, A., Joyce, N., Ganerød, M., Wijbrans, J., Ishizuka, O., He, H., Ramirez, A., Pfänder, J., Lopez-Martínez, M.,
845 Qiu, H. and Singer, B.: Interpreting and reporting $^{40}\text{Ar}/^{39}\text{Ar}$ geochronologic data, *GSA Bull.*, doi:10.1130/B35560.1, 2020.

846 Singer, B. S., Thompson, R. A., Dungan, M. A., Feeley, T. C., Nelson, S. T., Pickens, J. C., Brown, L. L., Wulff, A. W.,
847 Davidson, J. P. and Metzger, J.: Volcanism and erosion during the past 930 k.y. at the Tatara–San Pedro complex, Chilean
848 Andes, *Geol. Soc. Am. Bull.*, 109(2), 127–142, doi:10.1130/0016-7606(1997)109<0127:VAEDTP>2.3.CO;2, 1997.

849 Sonder, R. A.: Zur Geologie and Petrographie der Inselgruppe von Milos, *Zeitschr. Volc.*, 8, 11–231, 1924.

850 Spakman, W., Wortel, M. J. R. and Vlaar, N. J.: The Hellenic Subduction Zone: A tomographic image and its geodynamic
851 implications, *Geophys. Res. Lett.*, 15(1), 60–63, doi:10.1029/GL015i001p00060, 1988.

852 Stewart, A. L.: Volcanic Facies Architecture and Evolution of Milos, Greece, University of Tasmania., 2003.
853 Stewart, A. L. and McPhie, J.: Internal structure and emplacement of an Upper Pliocene dacite cryptodome, Milos Island,
854 Greece, *J. Volcanol. Geotherm. Res.*, 124(1–2), 129–148, doi:10.1016/S0377-0273(03)00074-X, 2003.
855 Stewart, A. L. and McPhie, J.: An Upper Pliocene coarse pumice breccia generated by a shallow submarine explosive
856 eruption, Milos, Greece, *Bull. Volcanol.*, 66(1), 15–28, doi:10.1007/s00445-003-0292-z, 2004.
857 Stewart, A. L. and McPhie, J.: Facies architecture and Late Pliocene – Pleistocene evolution of a felsic volcanic island,
858 Milos, Greece, *Bull. Volcanol.*, 68(7–8), 703–726, doi:10.1007/s00445-005-0045-2, 2006.
859 Traineau, H. and Dalabakis, P.: Mise en evidence d’une eruption phreatique historique sur l’île de Milos (Grece), *CR Acad*
860 *Sci Paris*, 1–38, 1989.
861 Vougioukalakis, G. E., Satow, C. G. and Druitt, T. H.: Volcanism of the South Aegean volcanic arc, *Elements*, 15(3), 159–
862 164, 2019.
863 Wendt, I. and Carl, C.: The statistical distribution of the mean squared weighted deviation, *Chem. Geol. Isot. Geosci. Sect.*,
864 86(4), 275–285, doi:10.1016/0168-9622(91)90010-T, 1991.
865 White, S. M., Crisp, J. A. and Spera, F. J.: Long-term volumetric eruption rates and magma budgets, *Geochemistry,*
866 *Geophys. Geosystems*, 7(3), 262–266, doi:10.1029/2005GC001002, 2006.
867 York, D.: Least squares fitting of a straight line with correlated errors, *Earth Planet. Sci. Lett.*, 5(C), 320–324,
868 doi:10.1016/s0012-821x(68)80059-7, 1968.
869